Titre: Title:	Morphological Changes of Vanadyl Pyrophosphate due to Thermal Excursions
Auteur: Author:	Sepideh Badehbakhsh
Date:	2021
Type:	Mémoire ou thèse / Dissertation or Thesis
Référence: Citation:	Badehbakhsh, S. (2021). Morphological Changes of Vanadyl Pyrophosphate due to Thermal Excursions [Mémoire de maîtrise, Polytechnique Montréal]. PolyPublie. https://publications.polymtl.ca/9170/

URL de PolyPublie: PolyPublie URL:	https://publications.polymtl.ca/9170/
Directeurs de recherche: Advisors:	Jaber Darabi, & Gregory Scott Patience
Programme: Program:	Génie chimique

POLYTECHNIQUE MONTRÉAL
affiliée à l'Université de Montréal

Morphological Changes of Vanadyl Pyrophosphate due to Thermal Excursions

SEPIDEH BADEHBAKHSH
Département de génie chimique

Mémoire présenté en vue de l'obtention du diplôme de *Maîtrise ès sciences appliquées*
Génie chimique

Août 2021

POLYTECHNIQUE MONTRÉAL
affiliée à l'Université de Montréal

Ce mémoire intitulé :

Morphological Changes of Vanadyl Pyrophosphate due to Thermal Excursions

présenté par **Sepideh BADEHBAKHSH**
en vue de l'obtention du diplôme de *Maîtrise ès sciences appliquées*
a été dûment accepté par le jury d'examen constitué de :

Daria Camilla BOFFITO, présidente
Gregory PATIENCE, membre et directeur de recherche
Jaber DARABI, membre et codirecteur de recherche
Ali SHEKARI, membre externe

DEDICATION

To my beloved parents,

My lovely brother, Sepanta

Thank you for your unconditional love,

endless sacrifices, and words of encouragement

Thanks for being such a wonderful family...

ACKNOWLEDGEMENTS

I would like to express my sincere gratitude to my research supervisor, Prof. Gregory Patience for his extensive support and guidance, motivation, and the opportunity to study under his supervision. It was a pleasure to work with him and I highly appreciate his supportive attitude.

I also would like to offer my deep gratitude to my research co-director Dr. Mohammad Jaber Darabi for his motivation, patience, recommendation, and academic support.

I would like to greatly appreciate Dr. Nooshin Saadatkhah and Prof. Olga Guerrero Prez for their academic recommendations, assistance, and cooperation.

Thanks to Prof. Daria Boffito and Dr. Ali Shekari for taking part in my thesis committee.

Special appreciations of my lovely friends, my colleagues in our research group and Polytechnique Chemical engineering Department's student and professors that helped me during Master program.

And last but not least, from the bottom of my heart, I would like to express my everlasting gratitude to my wonderful parents, and my amazing brother for the absolute support they have provided me throughout my entire life. Thank you Mami, Baba, Sepanta. You always stood by me in my best and worst times. You made my life so beautiful and meaningful. Words are powerless to express how much I love you.

RÉSUMÉ

L'hydrogénophosphate de vanadyle hémihydraté ($VOHPO_4 \cdot 0.5\,H_2O$) est le précurseur du pyrophosphate de vanadyle ($(VO)_2P_2O_7$) (VPP), qui catalyse activement plusieurs chimies oxydantes comme le n-butane en anhydride maléique (MA). Les réacteurs à lit fluidisé et à lit fixe sont utilisés commercialement.DuPont a partiellement pratiqué cette chimie dans un réacteur à lit fluidisé circulant (CFB) à 400 °C et 4 bar. Le procédé CFB était basé sur le concept de Mars van-Krevelen dans lequel le réseau solide contribue à la majeure partie de l'oxygène de la réaction. Cependant, pour atteindre des vitesses de réaction élevées, il fallait co-alimenter en oxygène trois ensembles de spargers chacun avec 926 buses. L'activité catalytique du VPP a chuté en moins d'un mois dans l'usine pilote tandis que dans des conditions contrôlées dans des installations de laboratoire, l'activité est restée constante jusqu'à 6 mois, avec peu de signes de désactivation. Alors que les propriétés morphologiques du catalyseur en laboratoire étaient essentiellement constantes dans l'usine pilote, la surface a chuté et une fraction des particules a changé de couleur du vert/gris au noir. Comme l'usine commerciale, DuPont a co-alimenté en oxygène pur par des buses dans l'usine pilote. Au fur et à mesure que l'oxygène de la buse se mélange au gaz de recyclage qui contenait jusqu'à 20 % de n-butane, la composition du gaz passe à travers l'enveloppe d'explosion. Lorsque la fraction massique de solides était faible à proximité des barboteurs, l'oxygène brûlait le n-butane et augmentait la température locale au-dessus de 700 °C, ce qui était suffisamment élevé pour noircir le catalyseur. De plus, la composition du gaz au niveau du tuyau d'échappement en aval du cyclone a également atteint les conditions de flamme froide et la température était donc suffisamment élevée pour noircir le catalyseur, principalement des fines. Dans cette recherche, nous avons noirci le catalyseur dans des conditions contrôlées pour se rapprocher des conditions de l'usine pilote et du réacteur commercial pour étudier les changements morphologiques du VPP. Nous avons également tamisé le catalyseur équilibré (VPP qui était dans le réacteur commercial depuis plus de 2 ans) en différentes fractions pour étudier la relation entre la taille des particules et les propriétés physico-chimiques. La fraction de particules noires était plus élevée pour les particules de moins de 45 µm de diamètre par rapport aux particules de plus de 90 µm : le pourcentage de particules noires était de 50 % pour les particules plus petites contre 20 % pour les particules de plus grand diamètre. Un analyseur thermogravimétrique TA-Q500 a chauffé le catalyseur frais à 800 °C sous azote et flux d'air. Le catalyseur VPP est devenu noir au-dessus de 710 °C dans l'air mais n'a pas changé de couleur dans l'azote.Il y avait une diminution à la fois de la surface catalytique et du volume des pores du catalyseur de 23 $m^2\,g^{-1}$ and 0.14 $cm^3\,g^{-1}$ to 12 $m^2\,g^{-1}$ and 0.09 $cm^3\,g^{-1}$ dans le catalyseur équilibré

en raison de l'effondrement de la structure VPO. La surface totale de la poudre noire est inférieure à celle du catalyseur frais et équilibré, ce qui est également dû à l'effondrement de la structure VPO. De plus, la densité de particules du catalyseur a augmenté de 1713 $\mathrm{kg\,m^{-3}}$ à 1959 $\mathrm{kg\,m^{-3}}$ en raison d'une perte de porosité. Au-dessus de 700 °C, de nouvelles liaisons se forment et la phase catalytique $(VO)_2P_2O_7$, qui est la phase principale du catalyseur équilibré, réagit pour former une nouvelle phase cristalline $VO(P_2SiO_8)$. Le catalyseur calciné avec une texture mate a des particules satellites sur la surface extérieure, tandis que les particules du catalyseur équilibré sont brillantes. Les particules sphériques précurseurs, calcinées et catalytiques équilibrées se transforment en particules irrégulières dans l'échantillon noir dans le TGA car il semble que toute la structure ait fondu, ce qui est différent de ce qui s'est passé dans le réacteur commercial et l'usine pilote. Tous les échantillons ont une enveloppe de silice qui recouvre la structure poreuse et certaines particules ont des noyaux creux avec des trous jusqu'à20 µm. La surface du précurseur et du catalyseur calciné était poreuse avec des pores uniformes (5000 grossissements) qui sont devenus lisses dans le VPP équilibré.

ABSTRACT

Vanadyl hydrogen phosphate hemihydrate ($VOHPO_4 \cdot 0.5\,H_2O$) is the precursor to vanadyl pyrophosphate, ($(VO)_2P_2O_7$) (VPP), which actively catalyzes several oxidative chemistries like n-butane to maleic anhydride (MA). Both fluidized bed and fixed bed reactors are applied commercially. DuPont partially practiced this chemistry in a circulating fluidized bed reactor (CFB) at 400 °C and 4 bar. The CFB process was based on the Mars van-Krevelen concept in which the solid lattice contributes most of the oxygen to the reaction However, to achieve high reaction rates required co-feeding oxygen in three sets of spargers each with 926 nozzles. The VPP catalytic activity dropped within less than a month in the pilot plant while in controlled conditions in laboratory facilities the activity remained constant for up to 6 months, with little sign of deactivation. While the catalyst morphological properties in the laboratory were essentially constant in the pilot plant the surface area dropped, and a fraction of the particles changed color from green/gray to black. Like the commercial plant, DuPont co-fed pure oxygen through nozzles in the pilot plant. As the oxygen from the nozzle mixes with the recycle gas that contained as much as 20 % n-butane, the gas composition passes through the explosion envelope. When the mass fraction of solids was low in the vicinity of the spargers, the oxygen would combust the n-butane and increase the local temperature above 700 °C, which was high enough to turn the catalyst black. Furthermore, the gas composition at the exhaust pipe downstream of the cyclone was also reached the cold flame conditions and so the temperature was high enough to turn catalyst black, predominantly fines. In this research, we turned the catalyst black under the controlled conditions to approximate the conditions of the pilot plant and commercial reactor study the morphological changes of VPP. We also sieved equilibrated catalyst (VPP that had been in the commercial reactor for more than 2 years) into different fractions to investigate the relationship between particle size and physio-chemical properties. The fraction of black particles was higher for particles less than 45 µm in diameter compared to particles greater than 90 µm : the percentage of the black particles was 50 % for the smaller particles compared to 20 % for the larger diameter particles. A Thermogravimetric analyzer (TA-Q500) heated fresh catalyst to 800 °C under nitrogen and air flow. The VPP catalyst turned black above 710 °C in air but did not change color in nitrogen. There was a decrease in both the catalytic surface area and pore volume of the catalyst from 23 $m^2\,g^{-1}$ and 0.14 $cm^3\,g^{-1}$ to 12 $m^2\,g^{-1}$ and 0.09 $cm^3\,g^{-1}$ in the equilibrated- catalyst due to the collapse of the VPO structure. The total surface area of the black powder is lower compared to both fresh and equilibrated catalyst which is also due to the VPO structure collapse. In addition, the particle density of the catalyst increased from

1713 $\mathrm{kg\,m^{-3}}$ to 1959 $\mathrm{kg\,m^{-3}}$ due to a loss of porosity. Above 700 °C, new bonds form, and the catalytic phase $(VO)_2P_2O_7$, which is the main phase of the equilibrated catalyst reacts to form a new crystalline phase $VO(P_2SiO_8)$. The calcined catalyst with a matte texture has satellite particles on the exterior surface, while the particles of the equilibrated catalyst are shiny. The precursor, calcined, and equilibrated- catalyst spherical particles turn to irregular particles in the black sample in the TGA as it seems that the whole structure melted, which is distinct from what happened in the commercial reactor and pilot plant. All samples have a shell of silica which covers the porous structure and some particles have hollows cores with holes up to 20 µm. The surface of the precursor and calcined catalyst was porous with uniform pores (5000 magnifications) that became smooth in the equilibrated-VPP.

TABLE OF CONTENTS

LIST OF TABLES

LIST OF FIGURES

LIST OF SYMBOLS AND ACRONYMS

LIST OF SYMBOLS AND ABBREVIATIONS

BET	Braunauer-Emmett-Teller analyzer
BJH	Barret-Joyner-Halender
CFB	Circulating fluidized bed
d_{p}	Average particle size, µm
EDX	Energy dispersive X-ray spectroscopy
PSD	Particle size distribution
P/V	Phosphhorous to vanadium ratio, molar
MA	Maleic anhydride
n	Number of experiments
SEM	Scan electron microscopy
T	Reaction temperature, °C
TGA	Thermogravimetric analysis
U_{mf}	Minimum fluidization Velocity
VPO	Vanadium phosphorous oxide
VPP	Vanadyl Pyrophosphate
V^{4+}, V^{5+}	Vanadium oxidation states
wt.	Weight percentage, %
XRD	X-ray diffraction
XPS	X-ray photoelectron spectroscopy

CHAPTER 1 INTRODUCTION

1.1 Vanadium phosphate catalyst

In many industrial processes with valuable products, vanadium based materials are used extensively as components of different catalysts[3]. Among these, vanadium-phosphorus oxides are one of the most significantly studied catalysts in terms of the scientific and practical points of view[3,8,9]. The structure and composition of vanadium phosphate catalyst can be affected by different factors such as gas-phase composition, activation temperature, thermal treatment time, and the P/V ratio[9,10]. Vanadium oxidation state and P/V ratio of V-O-P oxides are the main factors to change the catalyst performance[9,10]. Different P/V ratio in V-O-P oxides as well as the type of V-O building units connections (corner/edge) makes various types of surface oxygen sites[3]. Therefore, various well-characterized, crystalline vanadium phosphate phases with different vanadium oxidation state have been identified : 5^+ (phosphates γ, δ-$VOPO_4$), 4^+ (pyrophosphate $(VO)_2P_2O_7$), and 3^+ (monophosphate VPO_4)[3,8,9]. Oxygen atoms bond to the surface of these compounds in various ways ; they can bond singly as (V=O, P=O), or doubly as (V–O–V, V–O–P, P–O–P) or even triply coordinate to the atoms V or P[3]. One of the most important phases with the equal quantity of vanadium and phosphorus (P/V equals one) is vanadyl pyrophosphate $(VO)_2P_2O_7$—known as VPP—is transformed from vanadyl hydrogen phosphate hemihydrate precursor ($VOHPO_4 \cdot 0.5\,H_2O$) and is the active and selective catalyst in the oxidation of n-butane to maleic anhydride (MA)[3,8,9]. Bulk VPP, with a crystalline phase containing 104 atoms in total (16 atoms V, 16 atoms P, and 72 atoms O), has an orthorhombic crystal system with three lattice vectors as : a=7.725 Å, b=16.576 Å, and c=9.573 Å[3,11]. In the VPP structure, P–O tetrahedra are linked two pairs of V–O octahedra[3]. The two joined VO_6 octahedra by the edges and the pairs of connected octahedra by PO_4 provide a layer structure in the (1 0 0) plane of vanadyl pyrophosphate[3]. The V=O bonds within the octahedra pairs are in trans position and also the pyrophosphate groups connected the layers[3]. The surface of VPP consists of P=O and V=O groups. The P/V ratio on the surface of VPP indicates the total number of P=O and V=O groups[12].

Catalyst surface plays a vital role on reaction pathways by forming a surface-adsorbate bond, changing the surface construction, and then its penetration into the surface[3]. Interaction and bond formation with the reactant(s) are due to the electronic structure of the surface and the bonds change because of the adsorption and desorption processes[3]. Several studies have been conducted to evaluate the electronic structure of VPP surface especially the behavior

of the surface oxygen sites that coordinate in different ways and cooperate in the reactions that are catalytically active[3].

According to some studies by Ballarini and coworkers[13,9] the active surface of equilibrated catalysts varies with both the reaction conditions and the catalyst P/V ratio. They also investigated the reactivity of VPO catalysts with various P/V ratio under both steady and unsteady conditions[13].They observed formation of a selective and active surface which is like $VOPO_4$ at 320 °C, while it becomes less selective by increasing the temperature to 380 °C[13].

1.2 VPO properties

1.2.1 Reactivity of VPP

VPP has sites for the oxidative dehydrogenation of paraffins which is illustrated by formation of :

1. Benzene from cyclohexane with high specificity
2. Olefins and diolefins from n-paraffins
3. Cycloolefins from cycloparaffins
4. Aromatic compounds from decaline[14]

Also, this catalyst has centers which are able to perform with high specificity the allylic oxidation. Therefore, VPP does not produce olefins with considerable selectivity in the oxidation of paraffins[14]. It also has centers to insert oxygen into electron-rich substances and acid centers capable of performing various transformations[14]. One of the main properties of VPP is supporting biomolecular condensation reactions which are not acid-catalyzed but are catalyzed by the suitable geometry of sites which adsorb the molecules[15]. This property is significant in the formation of the phthalic anhydride precursor from intermediate pentadiene[15,16]. Another major property of this catalyst is its capability to simply go through structural changes which are reversible from $VOPO_4$ phases into $(VO)_2P_2O_7$ phase[15,17,18].

1.2.2 Role of acidity

The acidity of the catalyst is a key role in controlling the catalyst performance[19]. Some researchers examined the surface acidity of both equilibrated and non-equilibrated VPO catalysts[19,20]. For this purpose, they used ammonia, pyridine, and acetonitrile by the adsorption of which the presence of all strong Bronsted sites and medium strong and very strong Lewis sites on the surface of the catalyst was shown using Fourier transform-IR spectroscopy[19,20].

There is an increase in very strong Lewis acidity for the equilibrated catalysts with a better crystallized pyrophosphate[19]. The surface of all the VPO solids have strong Lewis and Bronsted acid sites in the different ratio[21,22]. The usual reduction in the Lewis/Bronsted ratio with temperature indicates that the Bronsted sites are stronger compared to the Lewis centers[19]. The Lewis and Bronsted acidity of the VPP make a significant contribution to the catalytic activity and selectivity of VPO[15,20,19]. It was reported by Centi and coworkers[23,20,9] that both Lewis and Bronsted acidity are significant in the selective oxidation of butane to MA. The interaction between V^{4+} and (P-OH) groups which are a Lewis acid sites and an acidic Bronsted site respectively, is needed to break the C-H bonds of n-butane[9,20].

1.3 Hydration and transformation of VPP

As we explained in the previous section, VPP as either pure phase or in conjunction with others phases such as $VOPO_4$, amorphous, phosphorus rich phases, is a common active catalyst for the n-butane oxidation to MA[3,8,9]. During this reaction, water is unavoidably formed as a by-product which can change the structure of the catalyst at high temperatures[24]. Some researchers[25,24] indicated that VPP in the presence of water is rehydrated to $VOHPO_4 \cdot 0.5\,H_2O$ when it is heated up to temperature around 140 °C for 24 h. The VPP catalyst can be affected by some parameters such as temperature, time and partial pressure of the water vapor[24]. Some studies that have been conducted in different temperatures and pressures, show formation of variety structures, and also water can change the structure of the catalyst during long term exposure in vanadyl pyrophosphate hydration reaction[24]. The reaction between VPP and water results in formation of some hydration products which significantly dependent on the reaction conditions[24]. In this reaction, the VPP transformation to the phosphorus deficient vanadium (III) phosphate is promoted by adding 1-propanol[24]. From the results, it is indicated that water plays a significant role in the phase composition of VPO catalysts and the phase structure of the active catalyst through long term use in an industrial reactor[24].

1.4 Activity of VPP catalyst

Guliants and coworkers[26] examined the vanadium phosphate catalyst systems which can be formed via various phases. They showed that the catalytic active phase is revealed as a active layer on the surface of the VPP catalyst and $VOPO_4$ phase is harmful to the performance of the catalyst[26]. Cavani and Trifiro[27] also suggest that V^{5+} phases have the responsibility to over-oxidize MA to carbon dioxide. Also, some other researchers illustrated that a redox

reaction is capable of formation of the V^{5+} phases which plays a significant role in the active catalyst[9].

Patience and coworkers[28] studied calcination and activation condition in vanadyl hydrogen phosphate hemihydrate transformation to VPP and investigated calcination experiments, different control variables including time, temperature, gas composition, pressure, and other effects on different parameter. The catalyst structure is affected by both the preparation method and activation procedure[9,28]. It should be considered in evaluating various activation techniques which are applied for several precursor preparation methods[9,28]. The changes during the activation process were investigated by researchers[9,28]. For this purpose, they heated the catalyst precursor until the reaction temperature in an n-butane/air and performed this process for a wide range of time duration[9].

1.5 Kinetics of VPP catalysis

MA is a significant intermediate which is mainly produced in the n-butane oxidation over vanadium phosphate catalysts[29]. This reaction is a dynamic process and some parameters such as time and operating conditions affect the VPO catalyst performance which may be due to a loss of phosphorus[29]. The importance of water on proper phosphorus distribution in the catalyst bed has been reported[29].

Many research studies have been conducted to investigate the kinetic of the n-butane oxidation and present a range of kinetic models[29]. Some researchers illustrated the kinetic of the reaction and dynamic behavior of the vanadium phosphorus catalysts in an industrial scale fixed bed reactor[29]. They reported that the optimum amount of phosphorus and water to the reactor feed ,permits control of both Temperature profiles and the rate of MA production[29]. Moreover, they presented a scheme for the dynamic and active surface of VPO catalyst which has a two-dimensional structure with different surface species which interconvert as a function of operating conditions[29]. Their proposed dynamic model compromise the two reactions as follow : a) slow phosphorus adsorption, and b) water adsorption reaching equilibrium faster and it is applied for a heterogeneous reactor model[29]. In their study, they observed that all the phosphorus and water related processes are entirely reversible and their presented reactor model is applicable of defining the changes of dynamic performance up to 400 h on stream[29].

1.6 VPO surface chemistry deposition of an amorphous V-P-O phase

In the past few decades, many studies have been conducted to investigate the deactivation mechanism of vanadium phosphorus (VPO) catalysts and prevent catalyst deactivation using metal promoters[30]. The deactivation mechanisms of the VPO catalyst can be a) amorphous phases crystallization b) the surface accumulation of carbonaceous species c) over-reduction or over-oxidation of vanadium d) loss of phosphorus e) agglomeration or sintering in a long duration oxidation[30].

Both optimum combination of V^{4+} and V^{5+} and P/V ratio moderately higher than 1.0, increase the activity and selectivity of the catalyst and the higher P/V ratio results in a lower catalyst over oxidation (V^{4+} into V^{5+})[30]. Moreover, the VPP catalyst can be deactivated by crystalline VPO_4 phases formation due to both extreme oxidation and high temperature caused by hot spot in reactors[30]. The VPO active sites as a thin amorphous layer exist on the top surface of $(VO)_2P_2O_7$[30]. This active site consists of dispersed V^{5+} on the surface of VPP or $VOPO_4$ microdomains which is coexisting with VPP phase[30]. Both the V^{5+} and V^{4+} oxidation states present high catalytic performance ;V^{5+} sites plays an important role in oxidizing the intermediates to form MA, while V^{4+} activates the n-butane[30]. The parameters such as preparation methods, activation, the nature of raw materials and other factors affect both the surface and bulk catalyst reactivity and the crystal morphology[30].

Some research studies[30] reactivated the catalyst by impregnation with a small amount of VPO (P/V= 0.86) phase and compared its catalytic properties and performance with the deactivated ones. For this purpose, they first eliminated the detrimental and harmful species like vanadium oxides, iron oxides, excess phosphorus, some forms of α-$VOPO_4$. Second, they suspended the used catalyst in a solution (isobutanol containing vanadium)[30]. During the treatment, an amorphous phase is formed adjoining vanadyl phosphate hemihydrate that cause surface reformation and the thin amorphous layer is formed by penetrating the species into the porous silica structure to rejuvenate the catalyst[30]. The results show that the V_2O_5 and β-$VOPO_4$ phases were removed, and the MA yield is increased over the reactivated catalyst during the reaction[30]. Moreover, MA selectivity and the rate of n-butane conversion of the reactivated catalyst improved compared to the used catalyst[30]. In addition, both V^{5+} / V^{4+} and P/V ratio are decreased due to treatment which does not require a heating step[30].

1.7 The preparation methods

1.7.1 VPP preparation

There are three main methods for VPP preparation that $VOHPO_4 \cdot 0.5H_2O$ is the only precursor phase[31].

— Standard aqueous HCl during a water extraction process
— V_2O_5 and H_3PO_4 reaction in isobutanol during a water extraction process
— $VOPO_4 \cdot 2H_2O$ and isobutanol reaction[14].

Recently, a different possible method has been developed to prepare VPP catalyst with a high specific activity per unit surface area in n-butane oxidation[31,32]. In this method, vanadyl hydrogenphosphate sesquihydrate ($VOHPO_4 \cdot 1.5H_2O$) is produced and activated during a redox reaction ($VOHPO_4.4H_2O$ reduction in 1-butanol) and at a specific temperature to prepare vanadyl pyrophosphate[31,32]. Also, a modified VPP catalyst can be produced by mixing sesquihydrate precursor and cobaltous acetate in 1-butanol[31,32].The specific activity of the cobalt-modified catalyst is high, but the presence of cobalt can decrease both surface area and the catalyst selectivity to maleic anhydride[31,32].

Hydrothermal synthesis of vanadium phosphate was prepared by some groups[9]. Pure VPP catalyst was obtained by heating $VOHPO_4$[9] . $\frac{1}{2}H_2O$ in a flow of N_2 at 750 °C for 72 h and it was oxidized by a flow of O_2 for between $0.5 - 24$ h[9]. Due to the presence of V^{5+} phases, all the pre-treated catalysts have higher selectivity compared to the pure VPP catalyst. However, the one hour oxidized sample has the highest selectivity to maleic anhydride[9].

By some Raman spectroscopy related studies, it was indicated that some phases like α_I-, α_{II}-, δ-, and γ-$VOPO_4$ can be hydrated to convert to $VOPO_4.2H_2O$ phase at room temperature[8]. In this process, the catalyst structure can be formed by the diffusion of the water into the catalyst lattice[8]. The α_{II}-$VOPO_4$ phase can be formed from the δ-$VOPO_4$ phase in a flow of n-butane/air around 400 °C[8]. On the other hand, the new formed phase- α_{II}-$VOPO_4$- is converted to γ-$VOPO_4$ phase in a flow of nitrogen by heating to the temperature around 700 °C and, the α_I-$VOPO_4$ phase can be formed from $VOPO_4.2H_2O$ when is heated to high temperature above 800 °C[8].

VPP formation from β-$VOPO_4$ which is considered as the most stable phase anhydrous orthophosphates, is also studied by some researchers[8,33]. They observed that β-$VOPO_4$ phase can be converted into $(VO)_2P_2O_7$ at the temperature around 400 °C in a flow of 1% 1-butene/air by applying in-situ laser Raman spectroscopy[8]. Some other researchers also reported a reversible β-$VOPO_4$ conversion to vanadyl pyrophosphate at a different temperature- around 500 °C- in a 2% n-butane/air flow[8].

As was mentioned in the previous paragraph, the β-$VOPO_4$ conversion to VPP can be reversible as well. This phase is transformed into β-$VOPO_4$ in the presence of oxygen by heating up to the temperature around 760 °C under the reactive conditions [8,33]. Some researchers [8,34] examined the behavior of VPP by environmental high resolution electron microscopy (EHREM) during steam treatment at a special temperature. They showed that deficiency can result in a disordered structure of the catalyst and a long-time calcination in steam can cause the material to become a different anion-lacking phase [8,34]. The kinetic study of catalyst revealed that both reactivity and selectivity of MA decrease significantly during steam treatment [8,34]..

Vanadyl phosphonates also can be synthesized and converted into VPP at considerably lower temperatures than $VOHPO_4 \cdot \frac{1}{2}H_2O$ and the surface area and the production rate of maleic anhydride increase in the prepared catalyst [9].

DuPont [8]prepared and synthesized VPO materials and $VOHPO_4.0.5H_2O$ in an organic media respectively : First, formation of $VO_2{}^+$ species was observed due to the reduction of V_2O_5 in a mixture of iso-butanol and benzyl alcohol and phosphorus was added as anhydrous H_3PO_4 [8]. Then VPP was transformed during the precursor calcination in air and activation in a flow of n-butane/oxygen/ nitrogen [8]. The role of transient operation condition on the VPO activity and conversions in a circulating fluidized bed (CFB) reactor for DuPont's process of n-butane oxidation become greatly considerable [8]. They studied the VPO phase transformation by exposing the catalyst under the operation conditions such as a cycle of oxidizing (oxygen/nitrogen) and reducing (n-butane/nitrogen) conditions [8]. In this study, the formation of different phases of vanadium orthophosphate was shown and characterization of VPO phase transformation under the transient conditions was studied [8]. These research studies indicate that VPP phase plays a significant role in industrial processes to form MA from n-butane [8].

CHAPTER 2 LITERATURE REVIEW

2.1 The industrial applications of VPO

VPP catalyst is known as a multifunctional catalyst which can be used in a variety of applications in industry[35]. This catalyst can be used for oxidation reactions such as a) the oxidation of n-butane to MA[36] b) the oxidation of n-pentane to maleic and phthalic anhydrides c) the oxidation of propane d) the ammoxidation of alkylaromatics and also f) the oxidation of different organic substrates in the liquid phase reactions in the presence of H_2O_2 and alkylhydroperoxides[35]. The surface acidity of the VPP catalyst plays a significant role in the mechanism of these reactions[35,19]. The acid and redox properties of this catalyst have a positive effect on some other application of VPP such as g) the oxidehydration of 1-butanol to maleic anhydride[37] and h) the oxidative dehydration of glycerol to acrylic acid[38]. In addition, this catalyst is used for the reactions with only the acid sites[35] . Some of the mentioned reactions along with other applications of VPP catalyst are described in the following :

2.1.1 Oxidation of n-pentane to maleic and phthalic anhydrides

The studies showed that n-pentane forms phthalic and maleic anhydrides using vanadyl pyrophosphate catalysts with the same selectivity in the n-butane oxidation to maleic anhydride[39,40]. The Langmuir-Hinshelwood mechanism defines the kinetic of this reaction[39]. Centi and coworkers introduced the kinetics aspects of the n-pentane transformation to phthalic and maleic anhydride over VPP catalyst with high activity and selectivity to clarify the reaction mechanisms and conditions in which the anhydride formation is improved[39,40]. The results showed four parallel formation reactions such as a) maleic anhydride, b) phthalic anhydride, c) CO and d) CO_2 as well as two other reactions- consecutive decomposition - for the two anhydrides transformation into the carbon dioxides[39]. Moreover, it is indicated that the phthalic anhydride is more selective for the reaction at both lower temperatures and concentrations of n-pentane or oxygen[39].

2.1.2 Oxidation of propane

Many studies investigated the partial oxidation of propane to oxygenates (e.g., acrolein and/or acrylic acid) on vanadyl pyrophosphate as a heterogeneous catalyst[41] . This heterogeneously catalyzed reaction as a challenging objective is considered by many researchers[41,42].Due to the environmental and economic aspects, this reaction is considered as an

alternative for the two-step synthesis in which propene is used as a primary material[41,42]. However, this reaction has some limitations such as low production rate at gas-phase conditions[41,42]. Vanadium phosphate are common materials for the selective O- and N-insertion reactions on aliphatics, methyl aromatics and methyl heteroaromatics[42,43].

2.1.3 Partial oxidation of toluene to benzaldehyde

The partial oxidation of toluene can form benzaldehyde which is the most important and simplest aromatic aldehyde in industry[44,43]. In the past few years, many researchers have been studied this reaction which occurs in the gas phase over the vanadium-containing catalysts to improve its performance[44,43]. Vanadium phosphorous oxides (V-P-O), especially VPP are common catalysts for the selective O- and N-insertion reactions on aliphatics, methyl aromatics and methyl heteroaromatics[42,43]. The researchers indicated that toluene can partially oxidized to transform into benzaldehyde over VPP catalyst[44,43]. The adsorbed species determined as a) cyclic anhydride b) water and c) benzaldehyde which is weakly adsorbed on the surface of the VPP catalyst by the aromatic ring[44]. However, the strong adsorption of benzaldehyde on the catalyst surface was detected at the temperature above 523 K during the reaction[44]. It was indicated that the acid hydroxyl groups produced by the water formation during the reaction improve both the benzaldehyde adsorption and oxidation reaction[44]. Moreover, high temperatures affect the total oxidation and higher selectivity of benzaldehyde improve the crystallinity of the catalyst[44,43].

2.1.4 Oxidehydration of 1-butanol to MA

A research study investigated the gas-phase transformation of 1-butanol into MA over various catalysts among which the vanadyl pyrophosphate have the highest selectivity to MA[45]. In the study, the performance of the two samples containing vanadyl pyrophosphate with different P/V ratio is compared to investigate the role of this ratio on the VPP catalyst behavior[45]. In the case of the prepared catalyst, they indicated that some factors play a significant role such as a) a controlled surface acidity is required for the formation of 1-butene from alcohol dehydration and b) mild oxidizing properties are necessary for the selective oxidation of the formed olefin[45]. They showed that the reaction over VPP catalyst as a selective and active catalyst can be performed as well as oxidation of both 1-butene and n-butane[45].

2.1.5 Vapour-phase dehydration of glycerol to acrolein

In the last few years, glycerol has been one of the demanding chemicals which is produced as a by-product of the biodiesel production[46]. Glycerol is converted to the valuable materials-acrolein- by a double dehydration reaction over a catalyst which is an alternative and economic process for the petrochemical ones[46]. Various materials and derivatives can be produced from acrolein as a raw and value-added chemical intermediate[47,48]. Many researchers have extensively studied the dehydration of glycerol over different catalysts among which V-P-O catalysts have strong acidic sites[46,49] as it is indicated that the surface acidity of the catalyst improve the activity for these reactions. Moreover, it is shown that[49] the uncalcined phases possess higher activity compared to the calcined phase and the calcination temperature have an impact on the Lewis acidity of the catalyst during the glycerol dehydration reaction. Some researchers synthesized and characterized a series of V-P-O catalysts with various P/V ratios to determine the catalytic properties of each samples in the gas-phase dehydration of glycerol[46]. They showed that the P/V ratio plays a significant role in the redox ability, acidity and finally the activity of the catalyst[46]. In addition, the catalyst is deactivated due to the coke formation and reducing the oxidation state of vanadium from V^{5+} phase to V^{4+}phase during the reaction[46].

2.1.6 Oxidative dehydration of glycerol

As was mentioned before, VPO is a selective catalyst in the oxidative dehydration of glycerol to acrylic acid due to its mild acid-basic properties[38]. In this reaction, molecular oxygen is added to prevent coke formation and decrease side reactions[38]. It is reported that[38] the acrylic acid production takes place in tandem-type reactors with glycerol dehydration and acrolein oxidation reactions in two reactors. A better heat balance can be found out by the integration of two reactions on one catalyst bed as the dehydration and oxidation reactions are endothermic and exothermic respectively[38]. The best result is obtained when the catalyst treatment occurs at 800 °C in which the rate of glycerol conversion and selectivity is high for useful products[38]. However, vanadium pyrophosphate oxides are less active compared to one-step formation of acrylic acid from glycerol[38].

2.1.7 Ammoxidation of ethanol to acetonitrile and the oxidation of β-picoline to nicotinic acid

Some researchers investigated the activity of the VPP catalyst for both these gas-phase reactions which can be considered as alternative processes to produce acetonitrile and nico-

tinic acid in industry[35]. They indicated that the reaction conditions of both n-butane and β-picoline oxidation to MA and nicotinic acid and are similar and also they predicted the similar active surface in both cases[35]. Regarding the ammoxidation of ethanol to acetonitrile, the reaction conditions is examined to be more reducing compared to the n-butane oxidation to MA which is due to the presence of ethanol and ammonia as the reactants that have a strong interaction with VPP catalyst[35]. In the case of β-picoline oxidation, the strong interaction between the catalyst and the reactants leads to some surface saturation[35]. In general, the bi-functionality features of the VPP catalyst, especially its strong acidity, plays a significant role in these reactions because it catalyzed the undesired formation of ethylene or because it strongly interacts with the reactants especially those containing N atoms, ammonia and β-picoline[35].

2.1.8 Hydrocarbons oxidation over vanadium phosphorus oxides

The oxidation of hydrocarbons plays a significant role in different chemical industries[50]. Various chemical products can be produced via the numerous alkanes oxidation with a reversible V^{4+} / V^{5+} redox cycle mechanism[51,50] . Many research studies have been conducted to investigate the hydrocarbons oxidation over different homogeneous and heterogeneous systems with various oxidants that confirms the importance of this subject[50]. Vanadium phosphorus oxides are the common effective catalyst for the numerous alkane oxidation such as cyclopentane, cyclohexane and so on[50]. Some studies[50] investigated the oxidation of cyclohexane over vanadium phosphorus catalyst with hydrogen peroxide that was shown VPO catalyst is highly active for the oxidation of alkanes especially the C_5-C_{10} cycloalkanes and it can be effectively reused for the reaction.

2.1.9 Carbohydrate dehydration into 5-hydroxymethylfurfural

Lignocellulose can be converted into some chemical compounds such as 5-hydroxymethylfurfural (HMF) as a valuable intermediate to produce various materials such as polyamides, biofuels and other chemicals and derivatives[52]. VPO catalysts with various phases and morphologies are heterogeneous catalysts that have been widely used for the oxidation reactions in industry[53]. Among all preparation methods, the synthesized VPP catalyst in organic media possesses more acid sites[52]. Some researchers investigated the dehydration of fructose and glucose which produce 5-hydroxymethylfurfural in the presence of a series of VPP catalysts supported on the surface of KIT-6 in the benzyl alcohol/iso-butyl alcohol mixture (or VPP/KIT-6 catalysts) to show the importance of surface area in the catalytic performance of different synthesized catalysts during the reaction[52]. They also determined the effect of

a) reaction temperature b) time c) the amount of catalyst and d) the amount of VPP on the support and some other parameters to obtain higher 5-HMF yield[52]. From the results, it was concluded that the VPP/KIT-6 catalysts have the best activity in comparison with the bulk of VPP and the catalyst is environmentally friendly because it can be simply recycled with a negligible change in its activity[52].

2.1.10 Ammoxidation of 3-picoline to nicotinonitrile

Many industrial companies and researchers studied ammoxidation of heteroaromatics over vanadium-containing oxides which used as supported, bulk, or multi-component catalysts[54]. The researchers[54], industrially synthesized bulk VPO samples in the ammoxidation of 3-picoline and VPO solids were used in the form of calcined, precursor and equilibrated material to be characterized with different techniques in order to show the precursor transformation to catalyst compound, vanadium oxidation states, structural and surface properties. The objective of this research was to fundamentally characterize the solid-state in a methodical and efficient procedure to perform basic solid-state characterization in a systematic way to obtain more knowledge about the catalytic performance[54]. The catalytic data showed that the catalyst precursor does not have a high performance which is because of the solid-state transformation of the hemihydrate precursor into an ammonium-containing VPO phase[54]. On the other hand, excellent results obtained by the calcined VPP with high selectivity and nicotinonitrile yields[54]. The equilibrated catalyst sample showed that the decrease in the catalytic performance is basically the results of both carbonaceous surface depositions and reduced vanadium species[54].

2.1.11 Oxyfunctionalization of light paraffins

VPP is also an efficient and selective catalyst for the oxyfunctionalization of light paraffins such as oxidation of ethane to acetic acid, oxidation of n-pentane to maleic and phthalic anhydrides, and also the oxidation and ammoxidation of propane to acrylic acid and acrylonitrile respectively[9,55,56,57,58,59,60]. The formation of acrylonitrile from propane ammoxidation was examined on various catalysts including $(VO)_2P_2O_7$ from which higher selectivity was observed in the reaction as well as the V-Sb-O system[57].

2.1.12 Formation of furan from butadiene

Centi and Trifiro[61] examined the formation of furan as a by-product from butadiene in which vanadium-phosphorus used as a catalyst. They observed the reaction of furan synthesis from

butadiene on VPP and showed that furan possess high selectivity only when it undergoes under the reaction at low conversion rate and O_2/butadiene ratios[61].

2.1.13 Partial oxidation of n-butane to MA

Hydrocarbon selective oxidation processes are prevalent in the industry and extensive research is being done on the direct oxidative conversion of lower alkanes due to their lower cost compared to olefins[62]. Among all the above mentioned reactions, the main industrial application of vanadyl pyrophosphate is the oxidation of n-butane to maleic anhydride[18,63]. VPP is the most active and selective catalyst in n-butane oxidation to MA in both fluidized bed and fixed bed reactors[18,63]. This catalyst with high selectivity has a unique ability in the transformation of n-butane to maleic anhydride. In this reaction, which is a 14-electron oxidation, eight atoms of hydrogen are abstracted ; three oxygen atoms are inserted, and a multi-step polyfunctional reaction mechanism occurs entirely on the adsorbed phase[18]. It is an industrial selective oxidation reaction that includes alkane activation[18].

Some research studies[64] proposed that VPP catalyst is significantly affected by two parameters : a) The reactor feed configuration and b) The sufficient amount of oxygen which is important for the optimal efficiency of the catalyst.

The partial oxidation of n-butane to maleic anhydride occurs when the vanadium-phosphorous-oxide catalyst is contacted with a mixture of n-butane and oxygen at the temperature around $350-420\,^{\circ}C$[64]. Vanadyl pyrophosphate is the active phase of the catalyst with the V^{4+} vanadium oxidation state[64]. There are other crystalline phases -known as $VOPO_4$ - on the catalyst surface which are connected with the active phase and representing the V^{5+} vanadium oxidation state[64].

The behavior of vanadyl pyrophosphate catalyst in partial oxidation of n-butane to maleic anhydride have been studied for several years[62,63]. Recently, many catalysis studies have been conducted to investigate this reaction and the properties of the active phase of the catalyst. However, the active phases of the catalyst and the role of oxygen species needs to be further studied[64].

The vanadyl pyrophosphate phase- $(VO)_2P_2O_7$ - and its oxidized forms- $VOPO_4$ - have a significant impact on the catalyst activity[64]. The lattice oxygen on the surface of the catalyst is selective to MA but the oxygen species moderately participate in the reaction[64]. Alternatively, Both loosely bound and surface adsorbed oxygen have an important role in the catalytic activity[64].

2.2 Dupont circulating fluidized bed reactor

DuPont designed a circulating fluidized bed technology (CFB) and used VPP as the catalyst for this reaction to improve the selectivity of MA[62,65]. In this reactor, the VPP catalyst is carried from reaction zone to regeneration zones and vice versa in order to keep the catalyst in the most appropriate oxidation state to gain higher selectivity[66,62]. The capacity of the VPP catalyst to provide adequate oxygen to the reaction zone is the key role for the CFB technology[64,62]. The lattice oxygen are highly selective and active to produce maleic anhydride from n-butane[67,68]. The high concentration of both butane and oxygen play a significant role in retaining high activity and selectivity[65]. The catalyst is transferred from a net oxidizing zone to a net reducing zone in a CFB[65]. The catalyst which covered in silica shell is reduced by n-butane in a transport bed/riser with a high concentration of n-butane and oxygen, and a fraction of the pyrophosphate was oxidized from the V^{4+} oxidation state to the V^{5+} oxidation state in an air fed fluidized bed regenerator[65,62] which is an oxidizing environment whereas, in the reducing environment, the V^{5+} is a source of oxygen for partial oxidation of n-butane to MA[65]. Schuurman and Gleaves[67] showed that keeping VPP in a high oxidized state increase the rate of production and maleic anhydride selectivity[63]. Moreover, catalyst oxygen treatment history or the presence of oxygen during reaction affect the production rate of maleic anhydride[63].

One of the main specifications of the CFB technology is the capability of the VPP to transmit oxygen from the oxidation zone to the reduction zone[63]. The maximum possible rate of production in a pure redox mode is defined by the amount of oxygen that can be integrated in the catalyst lattice[63]. But some studies[63,69,70,71] show that the capability of VPP in transferring oxygen is limited, therefore the overall rate of production in redox mode is low. It was also predicted by Wang and Barrteau[70] the maximum amount of oxygen that VPP catalyst can store[63].Some researchers added some oxygen to the flow of n-butane to minimize the catalyst over-reduction which results in an efficient and higher maleic anhydride yield[63].

2.2.1 Commercial plant configuration

The schematic diagram of DuPont's commercial CFB facility is shown in Fig. 1[2]. The main parts of the reaction section are a fluidized bed in turbulent regime and a riser through which the catalyst is moved to the regeneration zone where air re-oxidized the catalyst in a fluidized bed[62]. And ultimately, a standpipe transfers the oxidized catalyst to the fluidized bed reactor[63]. The solid particles enter the base of the fast bed through a standpipe and are carried upwards through the riser where the gas velocity is about $6\,\mathrm{m\,s^{-1}}$[62,72].The diameter

and height of the riser are 1.8 m and 25 m respectively, while the fast bed with a diameter of 4.2 m and a height of 11 m, possesses two sets of cooling coils and also three oxygen spargers with 926 nozzles per sparger [62]. The gas-powder mixture enters the stripper tangentially and most of the particles fall into the bed and move through the stripping coils, while the gas and some fines ascend through a heat exchanger and a cyclone afterward [62]. The rate of separation in the stripper is high enough so that the cyclone is never overloaded [62]. From the stripper with a 96 % stripping efficiency, the solid particles fall through a standpipe and enter an air-feed regenerator equipped with the horizontal cooling coils [62,72]. The regenerator reoxidizes the reduced catalyst which enters the standpipe leading to the fast bed afterward [72].

The CFB reactor has the following main features ; for instance, the reduction and oxidation zone are two separated sections that is the most important feature which cause feeding higher concentration of n-butane and increases the selectivity to maleic anhydride up to 90 % [64,66,62]. The other advantage of this reactor is that the operating conditions in the reaction zone can be independently-based optimized [66,64]. Despite the advantages of the CFB reactor, there are some limitations such as low rate of oxygen transferred by the catalyst which required the rate of catalyst recirculation to supply sufficient amount of oxygen for the reaction [64].

The effect of some elements such as temperature, pressure, composition and solid fraction were examined by some researchers to study their roles on the oxidation of n-butane/oxygen [62]. The determination of operating conditions is highly important to minimize the n-butane combustion and maximize the rate of maleic anhyrdide production which are the main objectives of their research studies [62]..

The active surface site of the catalyst during the reaction plays a significant role in both reaction mechanism and the kinetic modeling determination [64]. The n-butane activation on the surface sites of the catalyst determines the onset of the reaction and the intermediates species are transformed through the selective or non-selective pathways [64].

Moreover, it is reported that an appropriate ratio of V^{5+} and V^{4+} phases is required to have an efficient catalytic activity whereas some studies indicate that the presence of the V^{5+} species cause the catalyst to be highly oxidized [69,64]. The results of some research studies on the different reducing and oxidizing environment on the vanadium oxidation state through the reaction indicated the MA selectivity is highly decreased due to the formation of V^{3+} species under the fuel rich conditions [64?]. Some other researchers also confirmed the negative effect of the reduction of V^{5+} species on the selectivity of MA [73]. It is also reported that the sites with a high oxidation potential are more selective [64]

Moreover, the oxygen species as the essential source of the catalyst activity and selectivity play a significant role during the operating process in the CFB reactors [71]. Also, both the

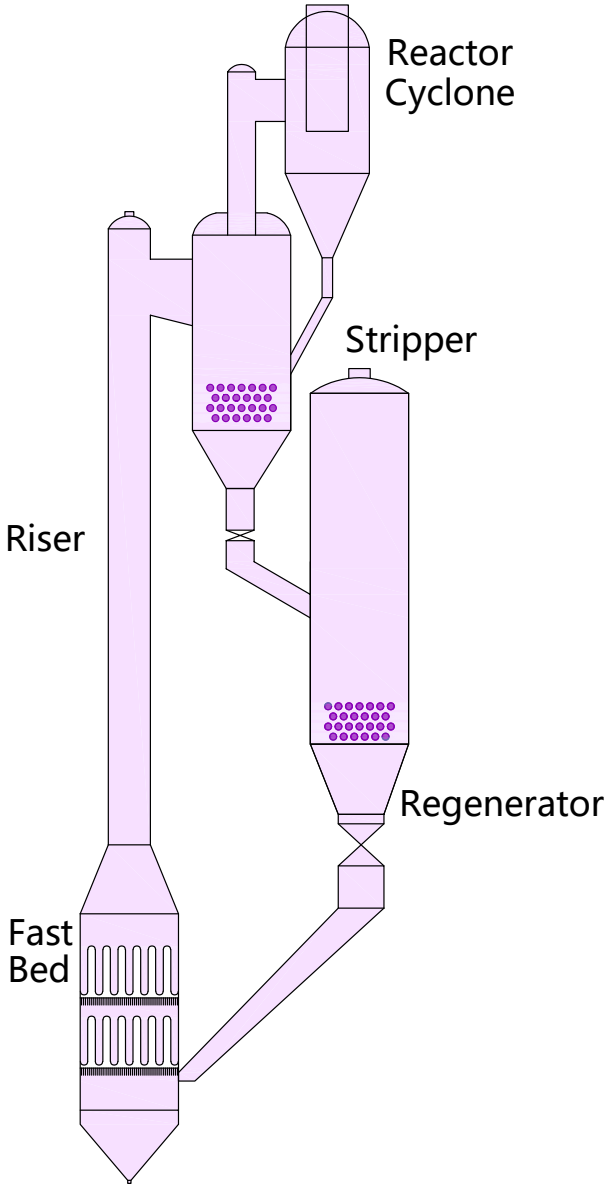

Figure 2.1 Circulating fluidized bed configuration for the commercial facility [2].

chemisorbed and surface oxygen on the catalyst surface as the essential sources convert n-butane to MA [71].

CHAPTER 3 PROBLEM IDENTIFICATION AND RESEARCH OBJECTIVES

3.1 Problem identification and Objectives

3.1.1 Problem identification

PROBLEM IDENTIFICATION AND RESEARCH OBJECTIVES It was shown in previous chapter that V-P-O catalyst could benefit many industries with valuable product. VPP catalyst is one of the most important phases of V-P-O compounds which is produced from vanadyl hydrogen phosphate hemihydrate precursor and it is a multifunctional catalyst which has various applications in industrial processes. The partial oxidation of n-butane to MA is the main application of VPP which is the most active and selective catalyst for this reaction. DuPont configured a circulating fluidized bed technology and used VPP for this reaction to improve the selectivity of MA.

VPP catalyst showed the constant activity in a lab-scale reactor over several months. However, it was deactivated to some extent in a pilot plant over a short period of time[62]. As a result, the surface area decreased, and a fraction of the catalyst changed color from green/grey to black.[62]. Independent thermal experiments in bench scale reactors resulted in the VPP catalyst to turn black when it was heated up to temperatures above 700 °C[62]. While, in the pilot plant, the typical operating temperature is about 400 °C[62]. Therefore, the mechanism of catalyst deactivation and color change of the catalyst to black was unclear. It is desirable to investigate the mechanism of catalyst deactivation and the parameters which cause the catalyst turn black.

3.1.2 Main objective

The general objective of this research is to identify the relationship between time, temperature, and oxygen on phase transformation of vanadium pyrophosphate which is the catalyst that partially oxidizes n-butane to maleic anhydride in a circulating fluidized bed reactor.

3.1.3 Specific objectives

The specific objectives of this research are to : a) Obtain controlled conditions to investigate the effect of both temperature and oxygen on the color change of the catalyst and b) Characterize the physical and chemical properties of the samples c) Determine the morphological

changes of vanadyl pyrophosphate catalyst due to thermal excursions during the reaction.

3.2 Plan of the dissertation

This Master's dissertation is divided into 6 chapters. Chapter 1 presents introduction and literature review. Chapter 2 presents the research objectives and plan of dissertation. In Chapter 3, we describe methodology which provides the experimental and analytical procedures. Chapter 4 presents the main results of this research in the form of a scientific article. Chapter 5 includes a general discussion. And finally, conclusion and recommendations are discussed in Chapter 6.

CHAPTER 4 METHODOLOGY

4.1 Methodology

In this section, we explain the material characterization techniques and experimental setup which have been used in this study. In addition, we explain the methods used to generate the black sample.

4.1.1 Materials

- Vanadyl pyrophosphate (calcined VPP) from DuPont
- The equilibrted-catalyst from DuPont
- Vanadyl hydrogen phosphate hemihydrate (VPO precursor) from DuPont
- The black sample which we generated under controlled conditions

The VPO precursor were synthesized on a commercial scale in an organic medium with isobutanol and benzyl alcohol. Then, it was micronized to 2.5 µm. Finaly, a porous silica shell was formed during spray-drying with polysilicic acid. The prepared VPP catalyst which is calcined and activated following the industrial protocols by DuPont Company consists of a vanadyl pyrophosphate phase and a silica shell that increases the attrition resistance[64,28]. It is noted that the equilibrated catalyst is the used calcined VPP after 2 years of commercial operation. This equilibrated catalyst contains some black particles that are deactivated which we generated in the laboratory in controlled conditions. We further explain the black sample preparation.

4.1.2 Experimental setup

According to the assumption that gas composition, temperature and time can cause the phase transformation of the catalyst and affect the color change of some particles to black, we prepared a experimental setup to obtain a controlled condition for black sample production. For this purpose, several experiments have been conducted by a) A furnace to heat up the catalyst under air in a crucible at different temperature ranges and time durations b) A setup with a reactor tube in a horizontal furnace to control the gas composition and temperature and c) A Thermogravimetric Analyzer (TGA Q 500). It should be noted that here the TGA setup had been used to produce black sample. We explain each experiment in the next section as follow :

4.1.3 Black sample preparation method

The equilibrated catalyst from DuPont contains some black particles which are deactivated. Hydrodynamic behavior of the particles is one of the main parameters in the performance of fluidized bed reactors. We assume that the particle size distribution could impact hydrodynamics of particles in a fluidized bed and the particle size might be correlated with the blackness of the equilibrated catalyst. Due to our assumption, we sieved the equilibrated catalyst into different fractions which confirmed this hypothesis. As you can see from Figure 1. the percentage of black particle in the equilibrated catalyst with smaller particle size less than 45 µm is higher than the sample with particle size larger than 90 µm. Thus, it is darker in color as well.

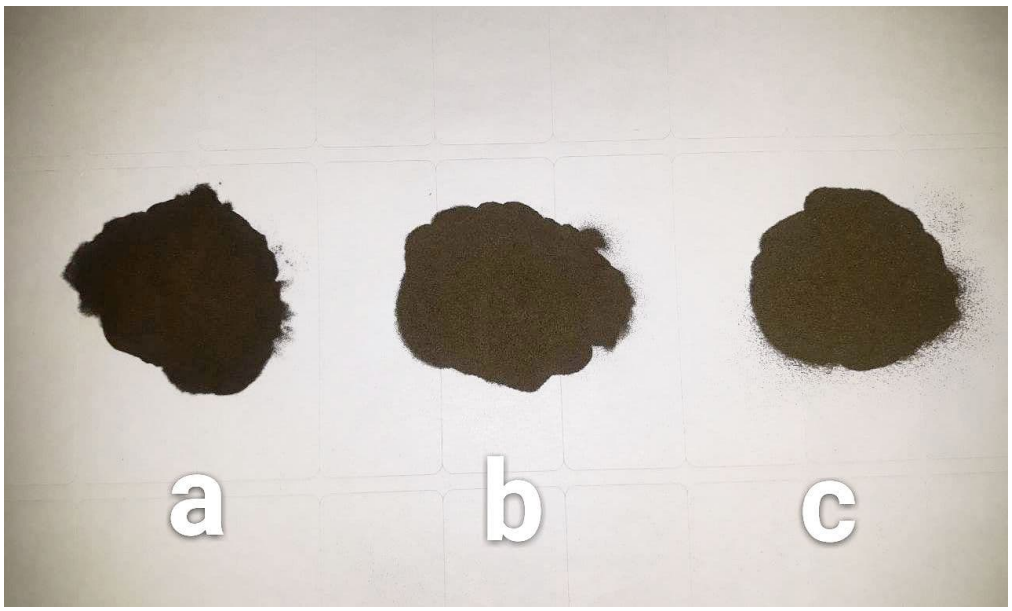

Figure 4.1 a) d_p <45 µm, b) 45 µm < d_p < 90 µm, c) 90 µm < d_p < 120 µm

We also sieved the calcined catalyst into different fractions and the detailed comparison of different particle size for both calcined and equilibrated catalyst is reported in the next chapter.

In order to get black sample, we tried to separate the black particles from the green ones in the equilibrated catalyst using a microscope which was unsuccessful due to the small size of the particles. Moreover, the percentage of the black particles in the sample was not high enough and it was tedious and cumbersome to separate them. Therefore, this methods was not practical and it was desirable to produce the black sample as follows :

First, we put the sample in a ceramic crucible and heated it up in a furnace for 2 h to the

temperatures ranging from 600 −1000 °C at a heating rate of 5 °C/ min. The catalyst changed color from green to yellow, brown, and dark brown at 600 °C, 800 °C, and 900 °C respectively. Moreover, the particles were sintered and turned from powder to one agglomerated block Figure 2. Therefore, we put the sample in a quartz reactor tube which was placed in a horizontal furnace and injected air into the reactor which was heated to 1000 °C at a heating rate of 5 °C/ min Figure 3. We observed only a few black particles and mostly green/brown particles that were stuck on the reactor walls that compromised the reactor integrity. In both procedures, the sample did not turn completely black which could be due to the insufficient oxygen in contact with the fresh catalyst and/or non-uniform heat distribution. To overcome these challenges, we used a Thermogravimetric Analyzer (TGA Q 500) which enable us to carry out the reaction under controlled conditions such as gas composition (i.e. air and nitrogen), temperature, and uniform temperature distribution (due to small sample size). For this purpose, TGA recorded the weight change of the sample as a function of both increasing temperature and time in a controlled atmosphere. We increased the temperature to 800 °C for 120 min at a heating rate of 10 °C/ min. The catalyst turned black in the presence of air under the above-mentioned controlled conditions Figure 4 . It should be noted that all the trials in inert atmosphere (nitrogen) were unsuccessful to generate black particles. This can confirm that oxygen is required to turn the catalyst black. Since the capacity of the TGA pan was around 0.1 g, we had to conduct the test several times to get enough black sample.

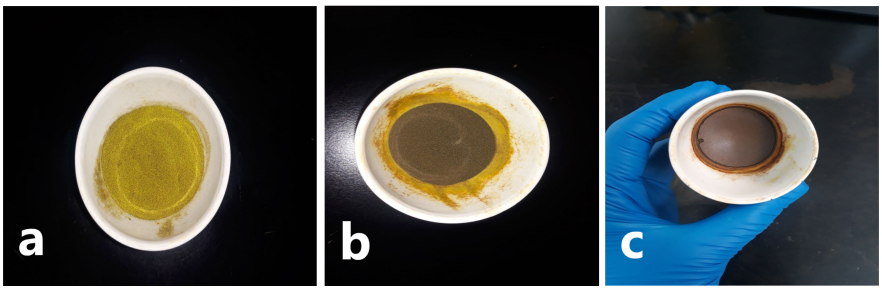

Figure 4.2 Heating the VPP calcined catalyst in a crucible to the temperatures a) 600 °C b) 800 °C c) 900 °C in a furnace

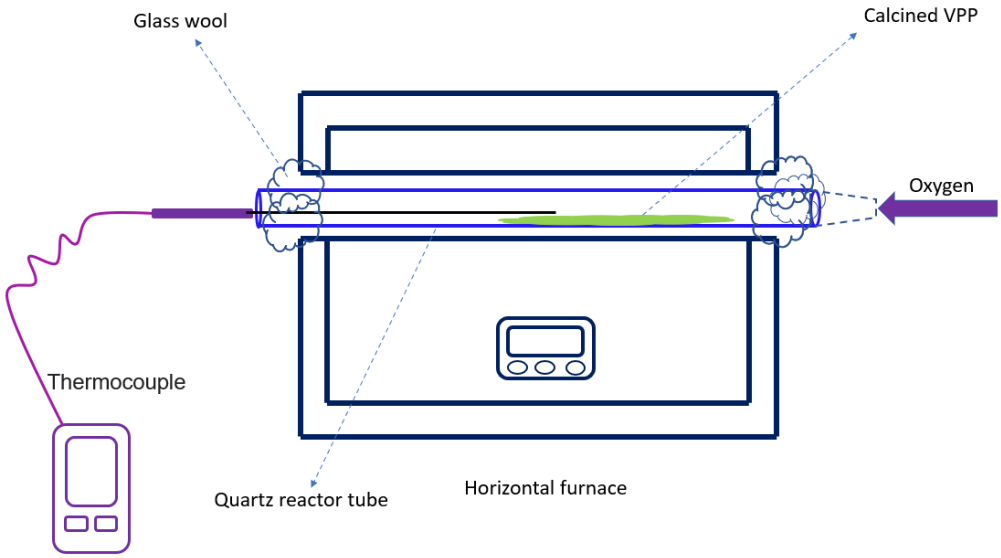

Figure 4.3 Setup-Horizontal furnace

Figure 4.4 Black sample obtained by TGA

4.1.4 Analytical and characterization methods

In this study, we measured the physical and chemical properties to investigate the morphological changes of VPP due to thermal excursions. We analyzed and characterized the samples as described below :

— Raman Spectrometry, X-ray diffraction (XRD) and XPS were applied to determine the molecular, crystallographic structure, and the phases of the samples as follow :
We applied an Invia Reflex Raman Confocal (RENISHAW) spectrometer as a long wavelength source to measure the Raman signals with the wavelength of 514.5 nm. The samples were treated in a mixture of 21 % oxygenin arogon 25, 100, 200 and 300 °C in a Linkan in-situ cell and a thermoelectrically cooled RemCam deep depletion (CCD) camera to record the spectra[74].
We recorded the X-ray diffraction patterns by an EMPYREAN PANanalytical diffractometer at ambient temperature via Cu K$\alpha_{1,2}$ (1.5406 Å) monochromatic radiation at 45 kV and 40 mA. We also scanned the diffraction angle between 5° to 80° for half hour with a detector PIXcel and Soller slits of 0.04 rad.
We applied a 5700C Physical Electronic X-ray photoelectron to analyze the surface chemistry with MgKα radiation of 1253.6 eV. All peaks were shifted with a reference to the maximum of the C1s peak at 284.5 eV[75].

— Nitrogen adsorption in an AUTOSORB-1 (Quantachrome Instruments, USA) measured the total surface area of the samples by the standard multi-point Brunauer-Emmett-Teller (BET). The samples were degassed at 200 °C overnight to evaporate the residual water. The pore size distribution was determined by desorption using the Barret-Joyner-Halender (BJH) method.

— The particle size distribution was determined using a laser scattering analyzer (LA-950 Horiba, China) by applying Mie algorithm.

— A Quantachrome Poremaster PM 33-12 measured both cylindrical pore volume and bulk density by the intrusion and extrusion curves over a dried degassed sample.

— An AccuPyc 1340 Folio Instrument with a chamber volume of 1, 3.5, and 10 mL measured the volume and density of the samples.

— High-resolution images of the samples, elemental analysis, and quantitative compositional information were obtained by a scanning Electron Microscopy / Energy Dispersive X-Ray Spectroscopy. This apparatus recorded P, V, and Si distribution in the powders. We mounted the particles on Technotherm 3000 and polished it with monocrystalline diamond suspension to observe the cross section of the particles.

— We applied an epsilon 4 benchtop EDXRF spectrometer to quantify silicon, phos-

phorus, vanadium, and iron in the samples. This apparatus has a silver anode x-ray tube, 50 kV excitation capabilities, a maximum power of 10 W, analyze elements non-destructivity.

— We measured the wight change of the sample by a Thermogravimetric Analyzer (TGA Q500) as a function of temperature and time in a controlled condition. The resolution is 0.1 µg and the accuracy is 0.1 %. The maximum load for the apparatus is around 0.1 g but loading more than 20 mg causes a decrease in the rate of mass transfer due to the sample shielding in the pan [76].

The basic principles of the analytical and characterization methods, which were employed in this study are described briefly as follows :

4.1.5 X-ray diffraction

X-ray diffraction (XRD) as a powerful and fundamental technique for advanced material characterization is applied to determine and quantify crystalline phases in materials [77]. In this method, a diffraction pattern which is a plot of the intensity vs. the angle of detector is measured in a wide range of 2θ to record all possible peaks [77,78]. The main concept of this method which is based on the diffraction of X-rays and detection of the diffracted signals, consist of X-rays, diffraction, and crystals [77,78,79,80].Bragg's law interprets the XRD phenomenon and calculate the diffraction as follow :

$n\lambda = 2d \sin\theta$

Where n is the order of diffraction, λ (nm) is the wavelength of the incident beam, θ in degree is the angle between the lattice planes and the incident beam, and d (nm)is the distance between the lattice planes of atoms for which the peak occurs [77,80]. X-ray diffraction is considered [77,78] as an effective characterization method which provide information on the crystallographic structure, chemical composition, and physical properties of materials. Power diffraction analysis determines the crystallinity, quality, and the quantity of different catalyst phases [77,80]. This technique provides valuable data on synthesis and catalyst deactivation due to structural transformation [77].

4.1.6 Particle-size distribution

The particle size distribution is measured by a light scattering method based on various theories such as Mie scattering theory, Fraunhofer diffraction theory, and Rayleigh scattering theory [81]. This method is characterized high resolution and accuracy, great variety of particle size measurement [81]. The Mie theory which has a higher precision than Fraunhofer, is more

appropriate to measure the particle size and it predicts the intensity of scattered light as a function of different parameters such as particle size, scattering angle, wavelength of incident light, and polarization of incident beam[81]. The Mie algorithm is applicable to measure the particle size in a wide range of particle types and it has a higher precision and resolution compared to other algorithms[81].

4.1.7 Mercury intrusion porosimetry

Mercury porosimetry is applied to characterize the porous materials[82]. This method is highly considered as a standard measure of total pore volume and pore size distribution in wide range of pore size[82,83]. The washburn equilibrium expression make a simple correlation between pressure and pore size as follow :

$P = \frac{-4\gamma \cos\theta}{d}$

where γ is the surface tension of fluid, P is the pressure, θ is the angle contact of the fluid, d is the capillary diameter[82]. Mercury porosimetry is the most popular time-tested method which is applied for both macropore and mesopore ranges and it is conceptually and experimentally faster and simpler than other methods such as calorimetry, thermoporometry, etc[82,83]. It quickly provides pore size distributions and is also employed for large pores $> 0.5\,\mu m$ which cannot be simply investigated by other methods[82,83].

The basis of mercury intrusion porosimetry is liquid intrusion into the capillaries under pressure and the expansion of mercury surface area during the initial intrusion includes irreversible and reversible intrusion[83]. The total porosity of the sample is calculated by the total volume of the liquid that is intruded[83].

4.1.8 Standard multi-point Brunauer- Emmett-Teller

The main concept of BET theory is associated with the gas adsorption on the surface of the materials[84]. This phenomenon is a physical adsorption caused by the van der Waals forces[84]. The amount of the adsorbed gas on the material surface determines the surface area and this adsorption process can be affected by temperature, pressure, etc[84]. The BET theory which is correlated with the Langmuir theory is based on a multilayer adsorption where there is no interaction between the layers which are as well in equilibrium[84]. The Langmuir equation is applicable for each layer and the BET equation is described as follow :

$\frac{(\frac{P}{P_0})}{n(1-\frac{P}{P_0})} = \frac{1}{n_m C} + \frac{C-1}{n_m C}(\frac{P}{P_0})$

Where n is the specific amount of gas that adsorbed at the P/P_0, P= pressure, P_0= saturation

pressure at the adsorption temperature, n_m = monolayer capacity of the adsorbed gas and C=BET constant [84].

4.1.9 Pycnometric density

Pycnometric density which is almost considered as true density is based on the nature and crystalline structure of materials and it is calculate by both molecular weight and crystalline lattice [85]. True density which is associated with the filled volume by material without porosity, is a main factor for characterization [85]. Density measurement plays a significant role in chemical synthesis and investigation of particle behaviour of a material under pressure [85]. Gas pycnometer provides the nearest approximation of true density by gas penetration into all pores to indicate the exact volume [85]. Helium pycnometer is easily and quickly operated to determine the volume of the material by specifying the gas pressure change [85]. Sample chamber with different size ranging $0.5\,\mathrm{cm}^3$ to $100\,\mathrm{cm}^3$ is accessible depending on available amount of material [85]. Therefore, by the measured material weight, the density can be calculated automatically [85]. The procedure of gas pycnometer includes two steps as a) Sample cleaning and air-moisture removing from the cell b) Exact volume measurement by the gas penetration into the cell [85]. The sample volume can be calculated by the following equation :

$V_{sample} = V_{chamber-cell} - \frac{V_{exp-cell}}{(\frac{Pr}{Pf})-1}$

Where $V_{exp-cell}$ (cm^3) is the volume of the cell which is expanded by the gas, Pr and Pf are the run fill pressure and final pressure (psig) respectively [85].

4.1.10 Raman spectroscopy

Spectroscopy is based on the interaction between the electromagnetic radiation and materials [86]. This method can include absorption, emission, scattering and fluorescence [86]. Various spectroscopic techniques which are applicable for both quantitative and qualitive analysis can characterize a wide variety of samples [86]. Raman spectroscopy as a reliable and multi-purpose method is used for the characterization of different type of materials and is the most effective method among all other spectroscopic techniques [86]. It is a scattering technique and performs the qualitive and quantitative analysis by determination of the frequency and intensity of scattered radiations, respectively [86]. In Raman spectroscopy, which is a scattering technique, a laser beam as a scattered light irradiates the material and the radiation interacts with the molecules and scatters in all direction [86] . As a result, the energy of atoms and molecules increase [86]. While a great deal of the scattered radiation has the same frequency as incident ones, only the light with a different frequency compared to the incident

light can provide a Raman spectrum[86]. The wavelength of incident radiation is important in Raman scattering method and a variety of lasers are applicable as light source which can be both short and long wavelength in Raman spectrophotometers[86].

4.1.11 Thermogravimetric analysis

Thermo- analytical technique is widely applied to provide information on physical and chemical phenomena and to characterize a system by determining changes in properties as a function of increasing temperature[87]. Thermogravimetric analysis as an experimental technique can be used for the reactions in which weight changes, and it presents the experimental results which is usually displayed as a curve by a) wight as a function of both temperature and time, b) Rate of loss weight as a function of temperature[88]. In thermogravimetric analysis, some elements can affect the curve shape such as the sample (weight, size, morphology), heating rate, the crucible geometry and atmosphere (air, argon, nitrogen ; pressure, humidity), gas flow etc[88,87]. This method is used investigate analytical procedures such as investigation of suitable weighing forms for various elements and also testing materials that are actual or potential analytical standards[88,87]. The reaction conversion (α), assuming that the weight loss is associated with a single reaction can be calculated as follow :

$\alpha(T) = \frac{\Delta m_T}{\Delta m_{tot}}$

Where Δm_T = weight loss at T, Δm_{tot} = step height[87]. This calculation method determines the conversion over the entire weight loss step[87].

4.1.12 Energy Dispersive X-ray Fluorescence

X-ray fluorescence (XRF) is a non-destructive compositional analysis and an emission spectroscopic technique which is based on the interaction of X-rays photons with material[89]. Each X-ray photon has a unique wavelength that can determine the concentrations of different elements present in the matter[89,90,91]. This qualitive and quantitative analytical technique is widely used in various fields and can provide information on material composition[91]. The X-ray interaction with the material can cause various phenomena such as emission of both characteristic X-rays and continuous X-ray[89,90,91]. XRF spectrometers are classified into two main groups as a) a wavelength dispersive (WDXRF) which detect the wavelength of X-rays photons and b) an energy dispersive (EDXRF) spectrometer which indicate the energy of x-rays photons[90]. Energy Dispersive X-ray Fluorescence (EDXRF) is an effective elemental analysis method with the ability to identify the presence of the different elements in the sample[90,91]. This apparatus requires an X-ray source, an X-ray detector, and a data acqui-

sition system[90,91]. In this technique, a lithium-drifted silicon crystal detector scatters the X-ray photons with different energy and determine their intensity[89,90,91]. Due to the lower energy of Si compared to the X-ray photons, it has the ability to excite the electrons to a higher energy state and the X-ray photon energies are separated and their intensity is determined by the detector[89,90,91]. The results are displayed as a graph of intensity as a function of energy[89,90,91].

4.1.13 X-ray photoelectron spectroscopy

X-ray photoelectron spectroscopy (XPS) as a powerful technique for physical surface analysis can provide valuable information on elements detection besides chemical bonding for a wide variety of materials[92]. This method can investigate the material surface layers or thin film structure which both are important in catalysis, corrosion, surface treatment etc[92]. In this method, XPS data is obtained from different specimen area and a concentric hemispherical analyzer measure the photoelectron energies emitted from the matter and provide a spectrum with a series peaks of which the binding energy identify each element and the peak areas characterize the surface material composition[92]. The photoemission process requires an optical excitation for the electron to be ejected from an orbital due to x-ray photon radiation and to be moved toward the vacuum level[92]. KE measurement of the emitted electron gives information on surface elemental analysis and the element chemical state[92]. The energy of a photon and KE of a photoelectron are calculated by the following relation :

$E = h\nu$

$KE = h\nu - BE$

Where KE is the kinetic energy of the electron, h=Plank constant and ν= radiation frequency, and BE is the required energy for electron ejection[92].

4.2 Article

As this thesis is article-based, all the results, discussions, and conclusions are presented in chapter 4 under the article entitled : “ Morphological changes of vanadyl pyrophosphate due to the thermal excursions ”.

CHAPTER 5 ARTICLE 1 : MORPHOLOGICAL CHANGES OF VANADYL PYROPHOSPHATE DUE TO THERMAL EXCURSIONS

Sepideh Badehbakhsh, Nooshin Saadatkhah, Mohammad Jaber Darabi Mahboub, Olga Guerrero Perez, Gregory S. Patience

Submitted to : Catalysis Today journal in July 2021

5.1 Abstract

Vanadyl pyrophosphate (VPP) is the active phase to convert n-butane to maleic anhydride in fixed beds, fluidized beds, and DuPont's circulating fluidized bed (CFB). The original CFB concept was based on the Mars van-Krevelen reaction mechanism in which the solid lattice contributes all of the oxygen to partially oxidize the n-butane. However, to achieve high reaction rates and selectivity requires the surface lattice to remain oxidized ; thus, DuPont co-fed pure oxygen through 926 nozzles at three levels in the reactor. Since pure oxygen was fed independently of the butane stream, the gas composition at the nozzle crosses the explosion envelope and the local temperature would rise. Furthermore, at the reactor exit downstream of the cyclone, the gas composition was within the explosion envelope. The temperature in these two locations were sufficiently high to turn the catalyst powder black. Here, we reproduced the high temperature conditions to examine the changes in catalyst morphology. A TA-Q500 heated the fresh catalyst to 800 °C under nitrogen and air flow. The VPP catalyst turned black above 710 °C to 720 °C in air. The catalytic surface area and pore volume of the fresh calcined catalyst decreased from $23\,m^2\,g^{-1}$ and $0.14\,cm^3\,g^{-1}$ to $12\,m^2\,g^{-1}$, and $0.09\,cm^3\,g^{-1}$ in the equilibrated catalyst due to the VPO structure collapse. Above 300 °C, new bonds form and the catalytic phase $(VO)_2P_2O_7$ transforms to a new phase $VO(P_2SiO_8)$ above 720 °C. The calcined spherical particles turn to irregular particles in the black sample. The porous surface of precursor and calcined catalyst with homogeneous pores became smoother in the equilibrated-catalyst (without any visible pores), and it turns to a rough non-porous surface in the black sample.

5.2 Introduction

Vanadium and phosphorus are prominent elements of many industrial selective oxidation processes[3,7,93]. VPO compounds form crystalline phases for which the vanadium oxidation state

varies from 5^+ (vanadyl phosphates γ, δ-$VOPO_4$), to 4^+ (vanadyl pyrophosphate $(VO)_2P_2O_7$), and 3^+ (vanadyl monophosphate VPO_4)[94,95,96]. The V-O-P phase and activity depend on vanadium oxidation state (5+, 4+, and 3+), the P to V ratio, the oxygen connection types at the edges, which dictate the catalytic performance,[3] and calcination/activation conditions. Oxygen coordinates at the surface as singly connected to V or P (P=O, V=O), double bridging (V–O–V, P–O–P, V–O–P), and triple bridging (V=O–P)[97,98].

The most selective phase is vanadyl pyrophosphate, $(VO)_2P_2O_7$ (VPP) that is produced from a topotactic transformation of the precursor—vanadyl hydrogen phosphate hemihydrate ($VOHPO_4 \cdot 0.5\,H_2O$)—at 390 °C in air[99]. Bulk vanadyl pyrophosphate creates an orthorhombic crystal layer with 16 V atoms and 16 P atoms with lattice parameters a=7.725 Å, b=16.576 Å, and c=9.573 Å[100,11]. A building unit contains two pairs of VO_6 octahedra joined together by PO_4 tetrahedra (Fig. 5.1)[3]. Adsorbates form bonds on the surface and penetrate into the lattice[3]. The electronic structure of the surface is the main reason for interaction and binding with the reactant(s). Several studies evaluated the electronic structure of the $(VO)_2P_2O_7$ surface, especially the behavior of differently coordinated surface oxygen sites at the surface of vanadyl pyrophosphate[3,12]. The activity of equilibrated catalysts varies with reaction conditions, phosphorous sublimation, which alters the catalyst P/V ratio, changing vanadium oxidation state, sintering, loss of surface area (due to localized hot spots), and poisons (sulphur accompanying the butane feed, for example)[13].

Vanadyl pyrophosphate catalyzes various classes of reaction with high selectivity and different steps have been proposed to characterize the mechanism to produce maleic anhydride from n-butane. (Table 5.1)[1]. Chemistries include oxyfunctionalization of light paraffins such as oxidation of ethane to acetic acid, propane oxidation to acrylic acid, propane ammoxidation to acrylonitrile, and n-butane and n-pentane partial oxidation of maleic and phthalic anhydrides[98,56,101,58,59,60]. It selectively dehydrates glycerol to acrolein due to its mild acid-basic properties but is less active in the one-step process to acrylic acid.[38]. Molecular oxygen reduces coke formation and minimizes side reactions[38]. Industrially synthesized and shaped vanadium phosphate performed poorly in the ammoxidation of 3-picoline due the solid-state transformation of the hemihydrate precursor into an ammonium-containing VPO phase. The calcined vanadyl pyrophosphate yielded nicotinonitrile up to 80 % as the selectivity approached 100 %. The equilibrated catalyst sample had poorer catalytic performance due to the reduced vanadium species and carbonaceous surface depositions[54]. $(VO)_2P_2O_7$ ammoxidizes propane to acrylonitrile and has been tested[101,93] to produce furan from butadiene[61].

The partial oxidation of n-butane to maleic anhydride remains the largest application of VPP[3,7,93] in both fluidized bed and fixed bed reactors[18,63]. The catalyst abstracts eight

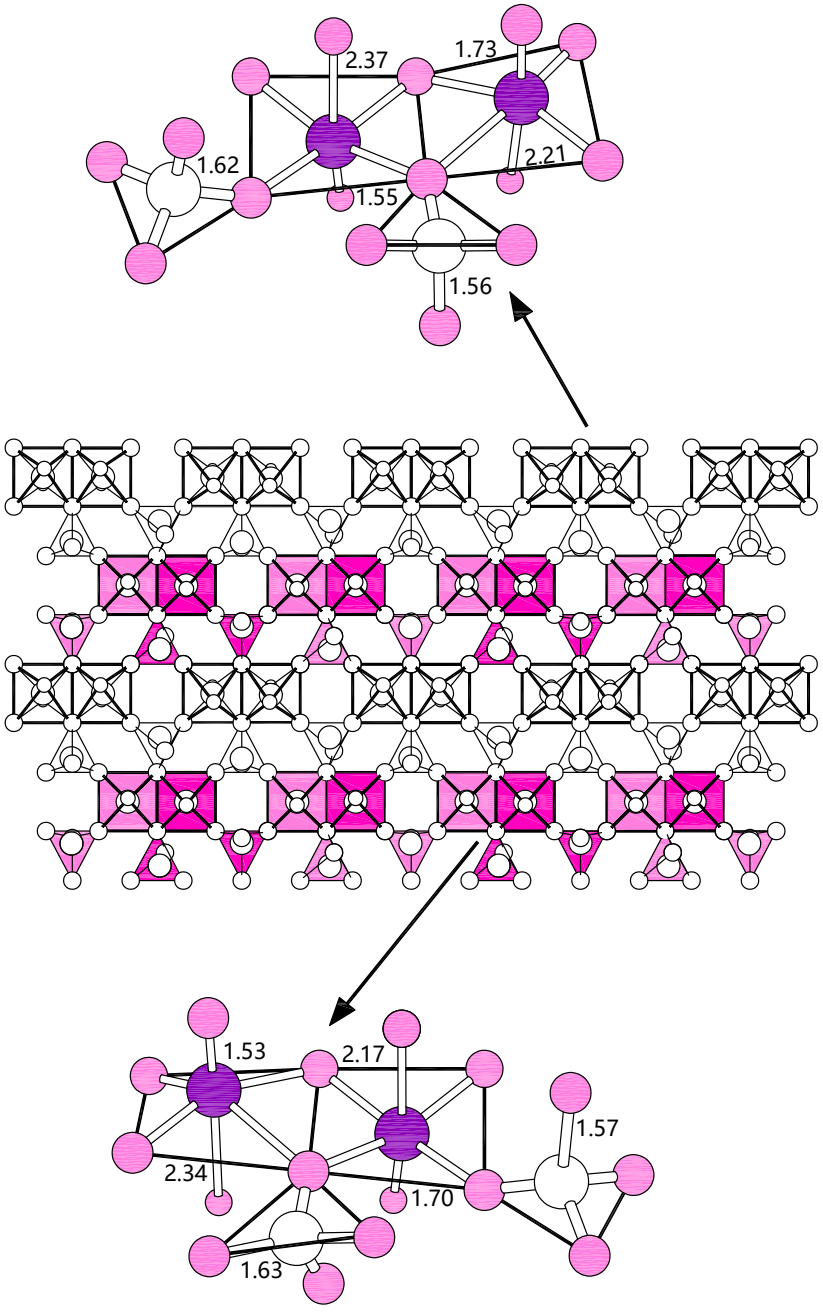

Figure 5.1 The $(VO)_2P_2O_7$ (100) structure. The purple and light pink circles refer to V and O atoms,respectively, while P centers are white. All distances in the figure are in Å[3].

Table 5.1 Classes of reactions catalyzed by vanadyl pyrophosphate[1].

Reaction type	Reactant	Product
Oxydehydrogenation	Isobutyric acid	Methacrylic acid
	Cyclohexane	Benzene
	Succinic anhydride	Maleic anhydride
	Hexahydrophthalic anhydride	Phthalic anhydride
	Paraffin	Olefin
Allylic oxidation : H-abstraction or O-insertion	Olefin	Diolefin
	2,5-Dihydrofuran	Furan
	Tetrahydrophthalic anhydride	Phthalic anhydride
Electrophilic oxygen-insertion	Benzene	Maleic anhydride
	Naphthalene	Naphthoquinone
	Furan	Maleic anhydride

atoms of hydrogen and inserts three oxygen atoms. This multi-step reaction mechanism occurs entirely on the adsorbed phase[18]. Fixed bed hot spot temperatures exceed 450 °C. DuPont commercialized circulating fluidized bed technology (CFB) that operated at 400 °C and 3 bar gauge at the exit (Figure 5.2)[102,2]. (The maximum operating temperature was constrained by the carbon steel vessel.) In this technology, the catalyst entered the base of the fast bed and was transported upwards to the riser at 6 m s^{-1}. The diameter and height of the riser were 1.8 m and 25 m, while the fast bed with a diameter of 4.2 m was 11 m tall and had two sets of cooling coils and three oxygen spargers with 926 nozzles per sparger (Fig. 5.2)[103]. The CFB transferred the catalyst from a net oxidizing zone to a net reducing zone[102,104]. In the air fed regenerator, a fraction of the surface vanadyl pyrophosphate species oxidized from the V^{4+} state to the V^{5+} state while in the fast bed, the n-butane reduced the V^{5+} species to V^{4+}.

VPO catalyst's surface has strong Bronsted sites, as well as medium strong and very strong Lewis sites in different ratios[105,21,22]. The vanadium oxidation state (acid sites) in the reaction condition controls the selectivity and activity of the catalyst[1] since the C-H bond cleavage on n-butane interacts with both a Lewis acid site (V^{4+}) and a Brønsted acid site (P-OH) on the surface of vanadyl pyrophosphate[93,106,15,107]. The Lewis/Brønsted ratio decreases with temperature[19]. The nature of V-P-O phases formed during the thermal treatment and in the operative condition determines the average oxidation state of vanadium[108,109]. Vanadyl pyrophosphate simply undergoes reversible structural changes from $VOPO_4$ phases into $(VO)_2P_2O_7$ phase[110,26].

Here, we characterized the precursor, fresh, and equilibrated VPP to identify phase changes,

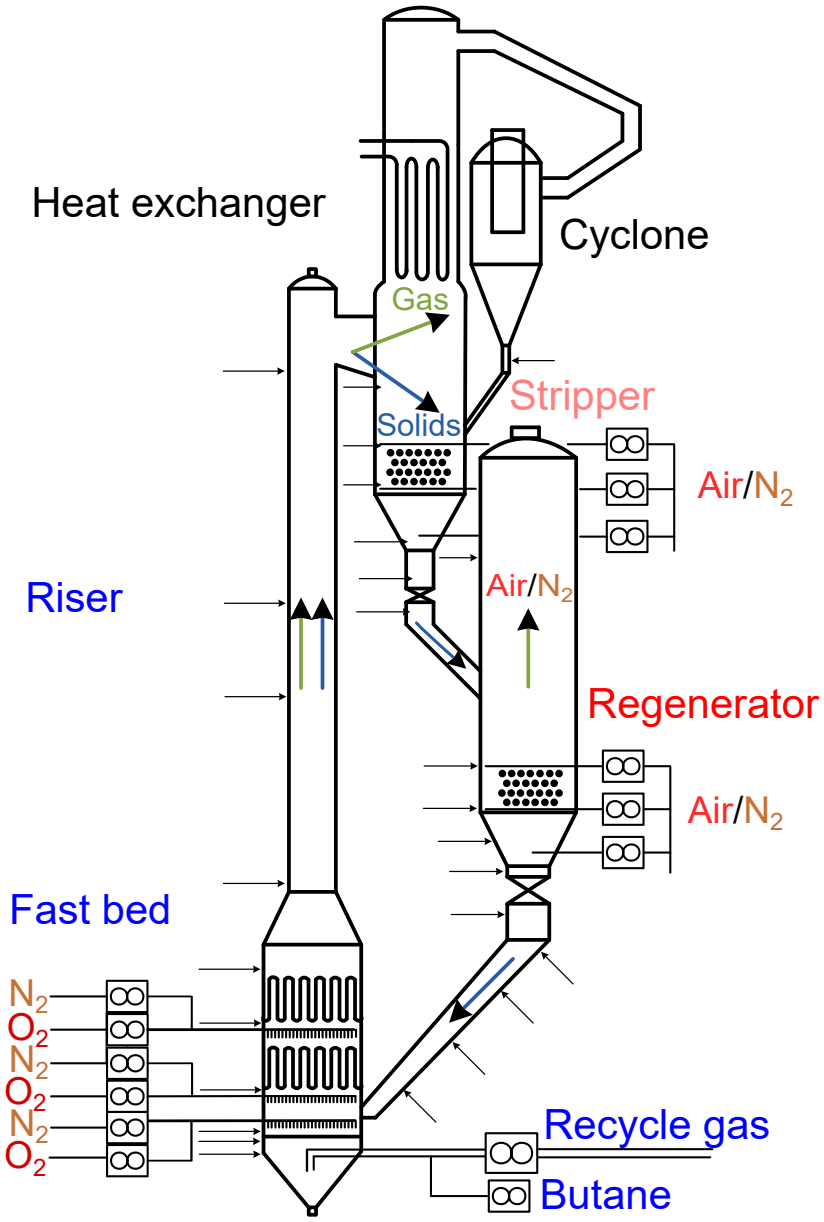

Figure 5.2 DuPont's commercial circulating fluidized bed configuration. A third oxygen sparger was added below the solids side entrance in the fast bed to maintain the catalyst at a higher oxidation state rather than allowing the butane/recycle gas to reduce the catalyst before reoxidation. The arrows represent pressure taps to measure catalyst inventory. The heat exchanger at the top of the stripper was added to reduce off gas burning that turned fine particles black. Air, nitrogen, recycle gas, and enriched air were possible gases to stip interstitial gas of n-butane and maleic anhydride. Steam failed as a stripping gas as it agglomerated the VPP Enriched air was fed to the regenerator to accelerate the reoxidation process. Reproduced from Patience[4]. Copyright Elsevier 2017.

catalyst structure deformation and catalyst deactivation formulation and phases. The equilibrated-catalyst was provided by DuPont.[111]

With this article, we recognize the tremendous contributions of Gary L. Rempel to the field of catalysis. His first published work in Web of Science Core Collection was from 1973[5] and he had been extremely productive with a median of almost 6 articles per year over 46 years. Over 1/3 of his articles mention catalysis as a keyword and most of this work has been dedicated to polymerization (Figure 5.3). As many as 8 of his articles mention maleic anhydride, which he applied to functionalize and rubber[112] and grafting it to natural rubber[113,114].

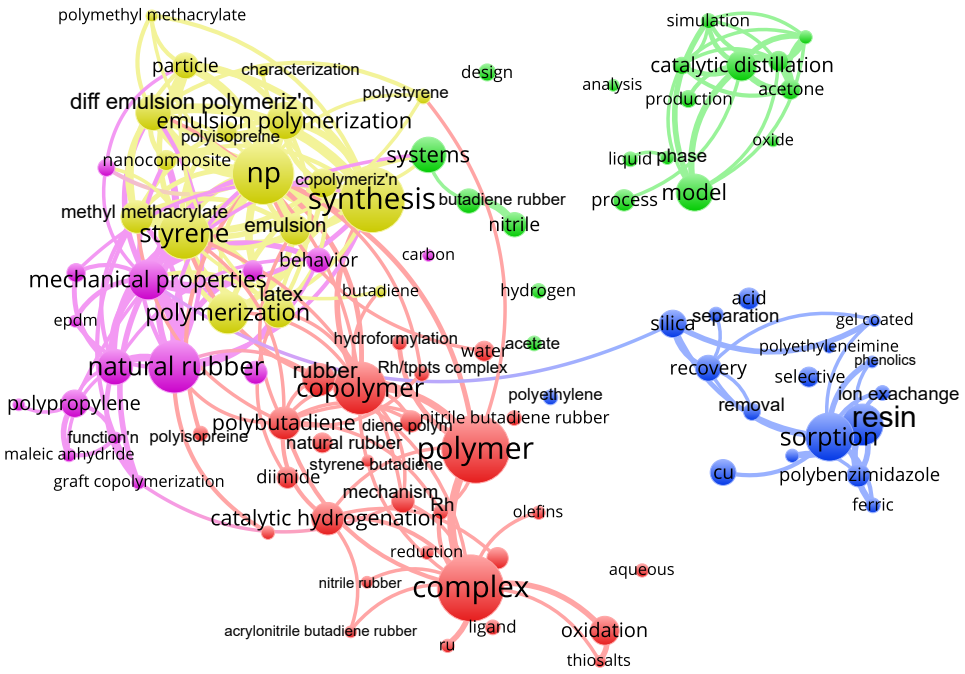

Figure 5.3 Keyword bibliometric map of the corpus of Gary Rempel's work from 1973 comprising 330 articles and 16 conference proceedings.[5,6]. The VOSViewer on-line program divides the 100 most common keywords into 5 clusters (same colour) where the size and font are proporotional to the number of articles that it appears : polymer (44 articles), model (22), sorption (31), synthesis(42), and natural rubber (34). The smallest circles for each category are thiosalts, (8), oxide (8) polyethyleneimene (8), polymethyl methacrylate (8), and functionalization(8). Lines represent citation links. Catalysis, with 120 occurences hydrogenation (79), and kinetics (66) were removed from the map because they dwarf the other themes so the circles would be too small to be noticeable.

5.3 Materials and methods

The two methods to produce VPP include :

1. An aqueous HCl method followed by a water extraction step ;
2. Reaction of V_2O_5 with H_3PO_4 in isobutanol and benzyl alcohol[14].

Patience at al.[99] synthesized the VPO precursor on an industrial scale in an organic environment with isobutanol and benzyl alcohol. A commercial micronized reduce the size of VPO particles from 1 µm to 2 µm, then the slurry was spray-dried with polysilicic acid which covers the VPO porous structure with silica shell. Spray-dried catalyst is less resistant than the activated catalyst but resistant enough to tolerate 100 h in the fluid bed[115]. Amoro's et al.[116] synthesized a series of vanadyl hydrogenphosphate hydrates (α-, β-$VOHPO_4.2H_2O$, $VOHPO_4.3H_2O$, $VOHPO_4.4H_2O$)(Fig. 5.4)[7].

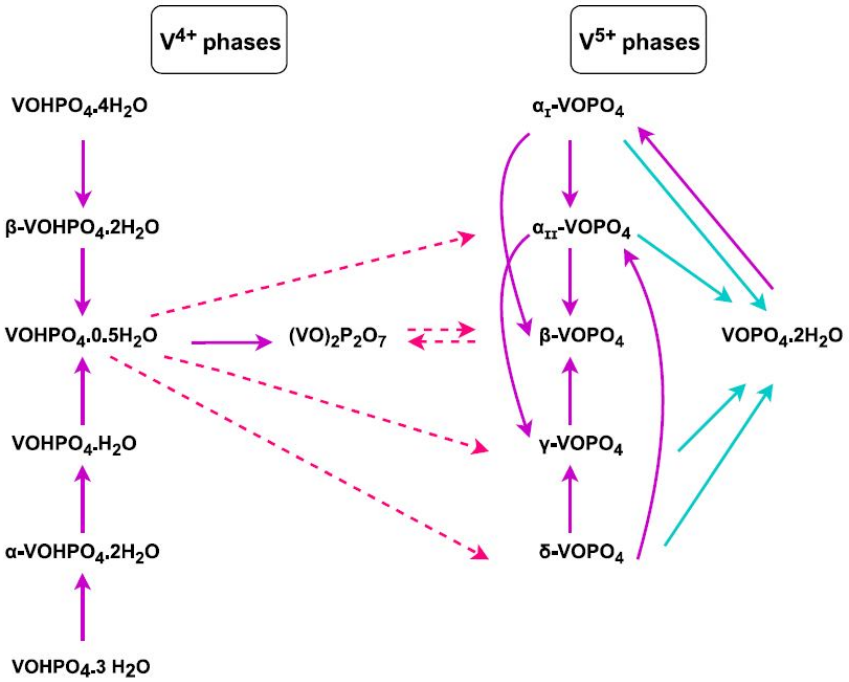

Figure 5.4 Diagram of phase transformations of VPO catalysts and precursors. The purple arrows refer to thermal treatment in nitrogen or air, the pink arrows refer to reduction in n-butane or oxidation in air, and the turquoise arrows refer to transformation in H_2O/air or H_2O/N_2 at RT[7].

To characterize the morphological changes between precursor, calcined catalyst, equilibrated catalyst, and black powder generated in the laboratory we applied several analytical techniques. We measured physical properties like the particle size distribution, surface area, minimum fluidization velocity (Table 5.2) and chemical properties with XRD, XPS, Raman, and EDS.

An EMPYREAN PANanalytical diffractometer recorded X-ray diffraction (XRD) patterns at

Table 5.2 Powder properties.

Property	Prec.	Calc.	Eq.	n	Comment
U_{mf}, $\mathrm{mm\,s^{-1}}$	9.4	4.1	3.8	3	$D_{\mathrm{t}} = 8\,\mathrm{mm}$
	905	898	1098	5	Scott density
ρ_{b}, $\mathrm{kg\,m^{-3}}$	913	913	1114	5	poured density
	997	1033	1259	5	tapped density
ρ_{p}, $\mathrm{kg\,m^{-3}}$	1551	2089	2018	5	particle density
		1915	2757	1	MIP
ρ_{p}, $\mathrm{kg\,m^{-3}}$		1713	1959	1	MIP
ρ_{sk}, $\mathrm{kg\,m^{-3}}$	2496	2739	2774	10	gas pycn.
A, $\mathrm{m^2\,g^{-1}}$		10.7	0.08	1	MIP
θ, $^\circ$	26	24	23	6	angle of repose
d_{p}, µm	88	67	59	3	Mean size
d_{p}, µm	79	59	55	3	Median size
s_{A}, $\mathrm{m^2\,g^{-1}}$	22	23	12	1	BET
	34	28	15	1	BJH
v_{pore}, $\mathrm{mL\,g^{-1}}$	0.11	0.14	0.09	1	BET
R_{pore}, Å	19.12	19.06	19.08	1	BET, BJH
O, $\mathrm{g\,g^{-1}}$	0.50	0.50	0.43	5	EDX
V, $\mathrm{g\,g^{-1}}$	0.24	0.22	0.27	5	EDX
P, $\mathrm{g\,g^{-1}}$	0.18	0.17	0.21	5	EDX
Si, $\mathrm{g\,g^{-1}}$	0.09	0.11	0.07	5	EDX
Fe, $\mathrm{g\,g^{-1}}$	0	0	0.03	5	EDX
V, $\mathrm{g\,g^{-1}}$		0.42	0.41	6	XRF
P, $\mathrm{g\,g^{-1}}$		0.09	0.08	6	XRF
Si, $\mathrm{g\,g^{-1}}$		0.03	0.02	6	XRF
Fe, $\mathrm{g\,g^{-1}}$		0.0	0.01	6	XRF

ambient temperature by Cu K$\alpha_{1,2}$ (1.5406 Å) monochromatic radiation at 45 kV and 40 mA. It scanned the diffraction angle between 5° to 80° for 30 min with a detector PIXcel and Soller slits (incident and diffracted beam) of 0.04 rad (Figure 5.11).

An LA-950 Horiba laser diffraction analyzer measured the particle size distribution (PSD) based on the Mie theory (Table 5.2)[117]. An AUTOSORB-1 (Quantachrome Instruments, USA) measured the surface area of the powder samples by the standard multi-point Brunauer–Emmett–Teller (BET). The samples were degassed at 200 °C to evaporate residual water overnight. The Barret–Joyner–Halender (BJH) method determines the pore size distribution by desorption isotherm. A Quantachrome Poremaster PM 3312 mercury porosimeter measure cylindrical pore volumes by intrusion and extrusion curves, over a dried degassed sample, up to 228 MPa and it covers a pore diameter range from 0.0070 µm to 1000 µm[118]. A Thermogravimetric Analyzer (TGA Q500) measured the mass change rate of the samples as a function of both temperature and time in a controlled atmosphere with a resolution of 0.1 µg and an accuracy of 0.1 %. The maximum load for the TGA Q500 is around 0.1 g, but loading more than 20 mg, decreases the mass transfer rate due to the shielding of sample on the pan.[76]. We measured volume and density of the samples by an AccuPyc 1340 Folio Instrument with three different chamber volumes (1, 3.5 and 10 mL) (Table 5.2).

An Invia Reflex Raman Confocal (RENISHAW) spectrometer equipped with a a RemCam deep depletion CCD detector of 514.5 nm Ar line, and a spectral resolution of ca. 1 cm^{-1} acquired the Raman spectra of the samples in the 200 cm^{-1} to 3200 cm^{-1} region. We treated the samples in a mixture of 21 % oxygenin arogon 25, 100, 200, and 300 °C in a Linkan in-situ cell to record the spectra[74]. An epsilon 4 benchtop EDXRF spectrometer quantified silicon, phosphorus, vanadium and iron in the samples. This spectrometer had a silver anode x-ray tube, 50 kV excitation capabilities, a maximum current of 2 mA and a maximum power of 10 W, analyze elements non-destructively.

A 5700C Physical Electronics X-ray photoelectron spectroscopy (XPS) apparatus analysed the surface chemistry of the samples with MgKα radiation of 1253.6 eV. We shifted all the peaks with a reference to the maximum of the C1s peak at 284.5 eV[75]. A field emission scanning electron microscope (FE-SEM-JEOL JSM-7600F) captured images at a voltage of 5 kV and an energy range of 10 keV. Scanning electron microscopy energy dispersive X-ray spectroscopy (SEM-EDS) recorded P, V, and Si distribution in the powders. To observe cross section of the particle, we mounted them on Technotherm® 3000 and polished it with monocrystalline diamond suspension.

5.4 Results and Discussion

The catalyst changed color during the synthesis process and in the CFB reactor. The precursor was dark green and turned pale green after calcination. Most of the calcined VPP was green but there were a couple of black particles per 100. The equilibrated catalyst had much less green and had many more brown and black particles (Figure 5.5) : as much as 50 % of the particles smaller than 45 µm were black while less than 20 % of the particles greater than 90 µm were black (Figure 5.6). Independent tests in bench scale reactors were capable of turning the vanadyl pyrophosphate black at temperatures above 700 °C.

In the initial stages of commisioning the commercial plant, more than 2 % of all the catalyst turned black due to back flow of n-butane up the regenerator standpipe. The temperature in this region was sufficiently high to deform the metal slide valve that was used to control the solids circulation rate (< 700 °C). An infrared gun reported an outside skin temperature on the metal standpipe greater than 500 °C during this event that lasted 9 h. To mitigate n-butane backflow, the commercial team built an insert that redirected the solids flow upward by about 30°, which solved the problem. The second area that caused black solids was the exhaust pipe in the region of the cyclone. The VPP powder effectively quenched free radicals thus minimizing the tendency to initiate thermal excursions but when the temperature was sufficiently not after the cyclone removed the solids from the stream and so the oxygen (< 4 %) would combust the n-butane and turn the entrained solids in the stream black. This problem was solved by installing a heat exchanger immediately above the stripper to drop the temperature by over 100 °C.

Both VPP color and activity remained constant in lab-scale reactors but activity dropped as the fraction of black powder increased in the pilot plant and the commercial reactor. Coincidentally with the drop of activity, the catalyst specific surface area decreased [102] and a fraction of the catalyst changed color from gray/green to black [2].

Over 100 thermocouples were positioned throughout the reactor in the fastbed at the sparger nozzle tips, in the standpipe, in the cyclones, and the exhaust piping but none of them ever recorded temperature rises of this magnitude. Sudden changes in the local temperature in the fast bed were as much as 40 °C, but more often the dozens of thermcouples positioned at the nozzles tips recorded temperature rises on the order of 2 °C [2,103]. In the pilot plant demonstration, catalyst also turned black due to thermal excursion at the sparger tips. Thermcouples positioned at the tips recorded instantaneous temperature rises of 1 °C to 10 °C and these were accompanied by a simultaneous drop in oxygen concentration and an increase in carbon dioxide (often < 1 %).

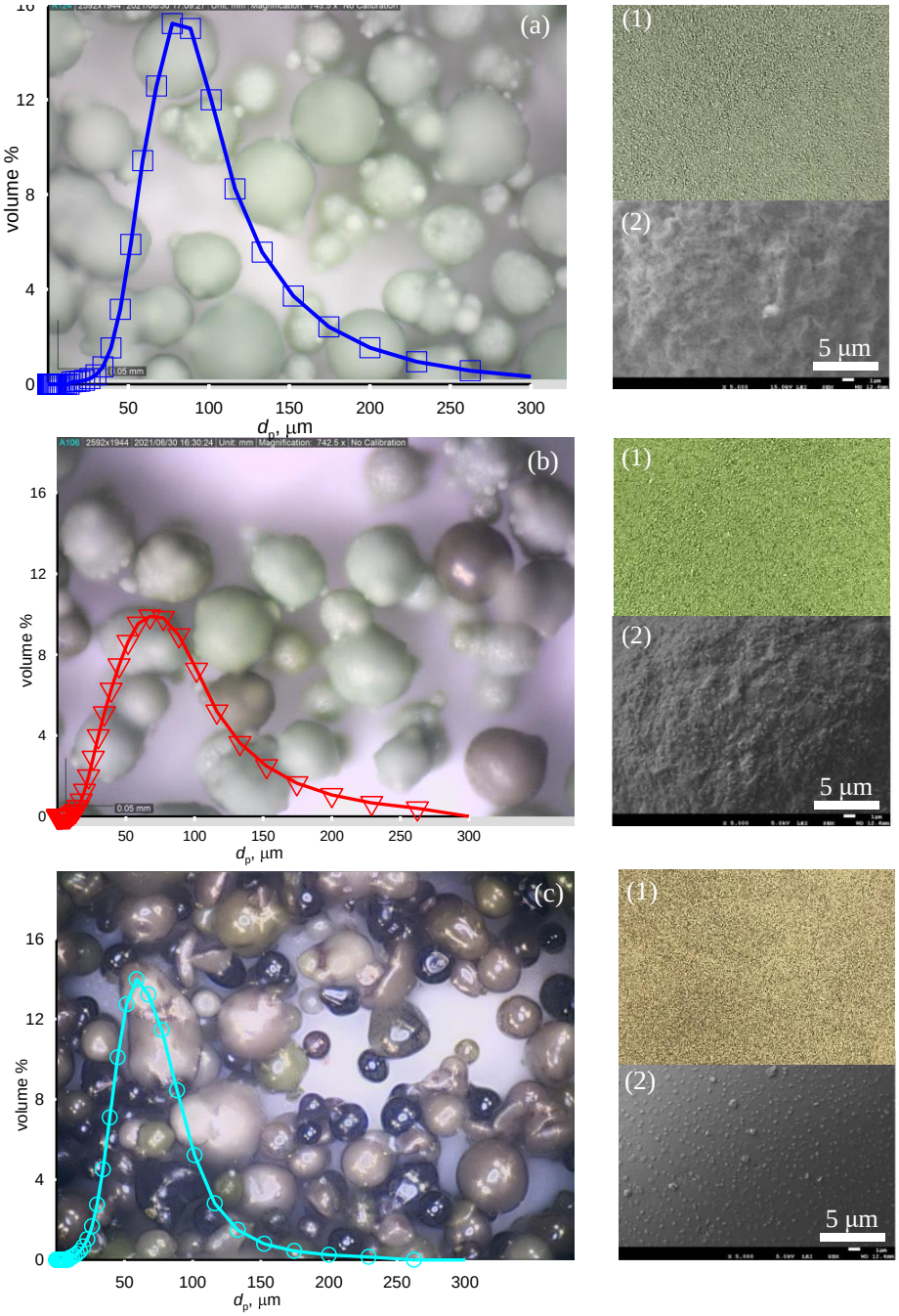

Figure 5.5 Microscope images of (a) precursor : (1) without any magnification (2) SEM image of the surface (b) calcined : (1) without any magnification (2) SEM image of the surface, and (c) equilibrated catalyst : : (1) without any magnification (2) SEM image of the surface

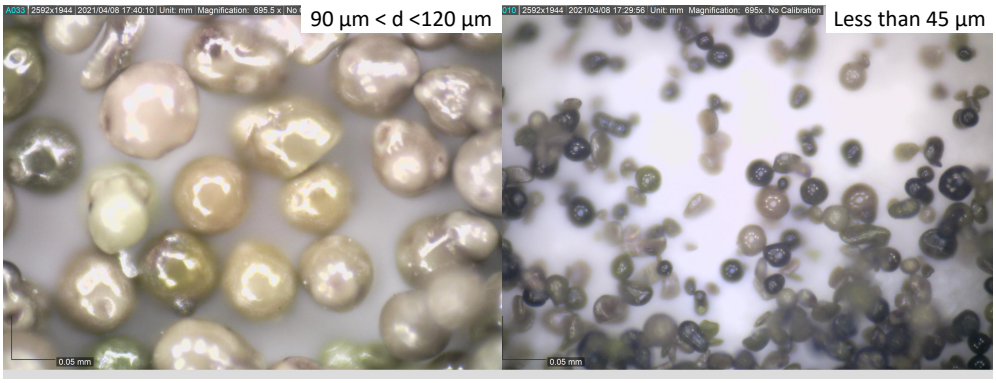

Figure 5.6 Microscope images of equilibrated catalyst : 90 µm $< d_p <$ 120 µm (left panel), d_p <45 µm (right panel).

The mean particle size of the precursor was highest at 88 µm, followed by to 67 µm for the calcined VPP, and to 59 µm for the equilbrated catalyst (Table 5.2). The calcined VPP had the broadest particle size distribution. Both the precursor and calcined VPP have satellite particles attached to the exterior surface that cleaved in the reactor as the catalyst circulated in the loop at over 4 kt h^{-1}. The images of the equilbrated VPP are very shiny : the white outline of each particle is reflected light from the lamp illuminating the surface. Both the precursor and calcined catalyst have a matt texture and so the reflected light is more dispersed.

The minimum fluidization velocity (U_{mf}) of VPP calcined and equilibrated-catalyst are 4.1 mm s^{-1} and 3.8 mm s^{-1}. VPO precursor has the highest U_{mf} among the three samples at 9.4 mm s^{-1}. In the black sample, the VPO structure collapsed resulting in a lower total specific surface area compared to both fresh and equilibrated-catalyst.

5.4.1 Physical characterizations

SEM-EDX detected vanadium, oxygen, phosphorus and silicon in all three catalysts (Table 5.2). The weight percent of both oxygen and silicon dropped during partial oxidation of n-butane to maleic anhydride, while the weight percent of vanadium and phosphorus increased moderately. Only the equilibrated-catalyst contains Fe. In the black samples, the main structure was obviously collapsed resulting in irregular particles(Figure 5.5).

Precursor, calcined and equilibrated samples all have a shell of silica (Figure 5.7 and Figure 5.8) covering a porous structure Some particles have hollow cores with holes up to 20 µm.

VPP and VPO precursor have higher BET and BJH surface area and pore volume compared

to the equilibrated-catalyst (Table 5.2). Both specific surface area and pore volume of VPP decreased from $23\,m^2\,g^{-1}$ and $0.14\,cm^3\,g^{-1}$ to $12\,m^2\,g^{-1}$ and $0.09\,cm^3\,g^{-1}$ in equilibrated-catalyst. The desorption path differs from the adsorption path, creating a hysteresis loop type H3 (Figure 5.9). The loops of type H3 typically exists in solids consisting of aggregated non-rigid plate-like particles[119].

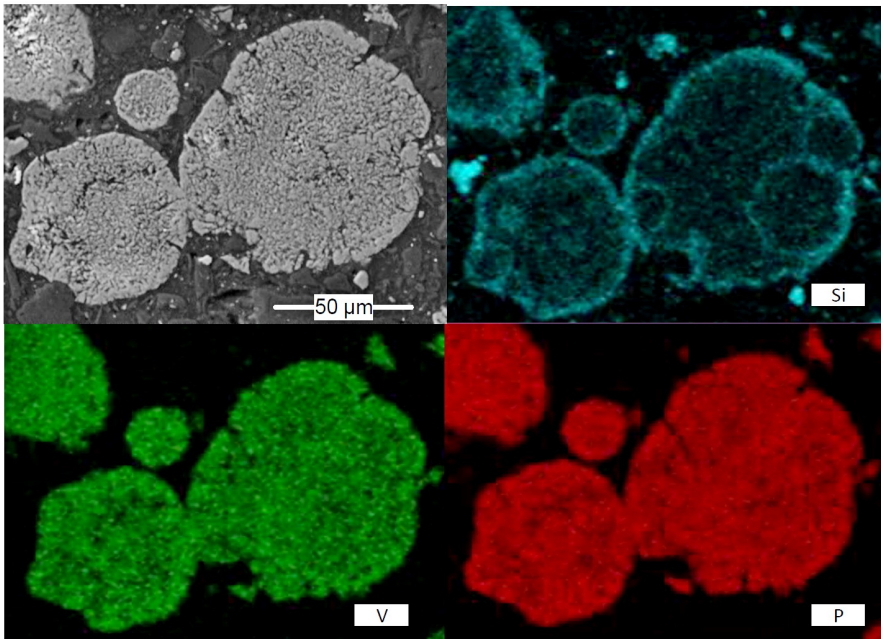

Figure 5.7 EDS elemental mapping of the calcined catalyst

The total surface area of VPP calcined is much higher than that of the equilibrated-catalyst, while both particle density and the bulk volume of the equilibrated-catalyst are higher compared to VPP calcined (Table 5.2). This suggests that during partial oxidation of n-butane to maleic anhydride, the total specific surface area decrease significantly, while the particle density increase slightly due to a loss of porosity.

5.4.2 Chemical characterizations

We heated all three samples in both nitrogen and air at a heating rate of $10\,°C\,min^{-1}$ until 800 °C followed by an isothermal hold of 30 min in TGA (Figure 5.10). Up to 400 °C, all samples undergo the same weight change pattern and lose weight in both air and nitrogen (loss of water). Above 400 °C in air, all the catalysts begin to gain 2 % mass, but in nitrogen, they continue to lose weight at a slow rate. All the samples turned black in air, but not in nitrogen.

In air, with increasing temperature up to 400 °C to 600 °C, all three samples lost mass, then

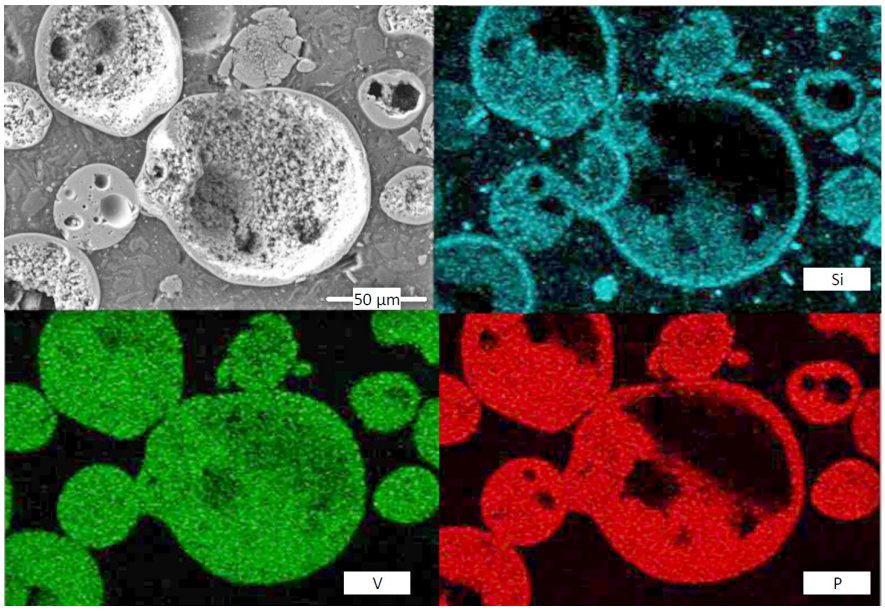

Figure 5.8 EDS elemental mapping of the equilibrated catalyst

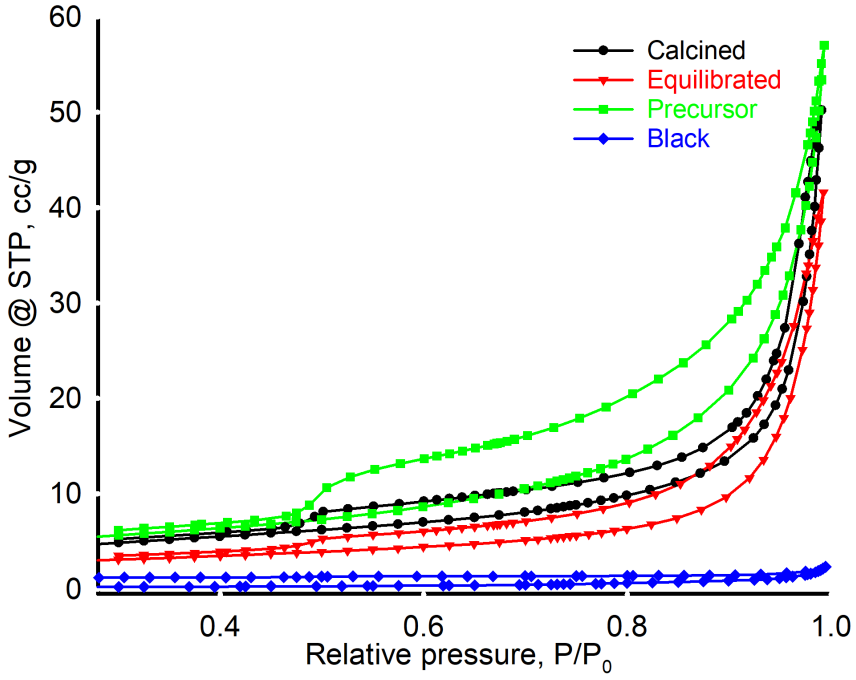

Figure 5.9 N_2 adsorption-desorption isotherms of VPP calcined, equilibrated-catalyst and VPO precursor

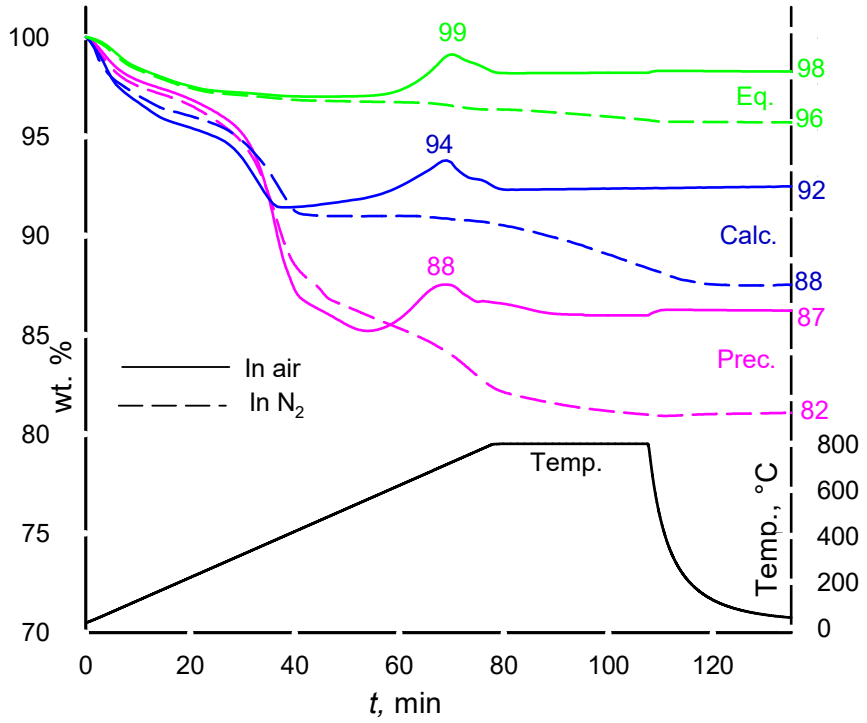

Figure 5.10 TGA analysis for VPP precursor, calcined, and equilibrated catalyst in air and nitrogen

slightly increased reaching a maximum at around 700 °C and then the mass dropped again until it stabilize at 800 °C (98.3, 92.5, and 87 % for equilibrated-catalyst, VPP calcined, and VPO precursor, respectively).

We associate the first mass loss to evaporation of physisorbed and chemisorbed water. The increase in mass around 700 °C happened only in air which is due to the oxidation of vanadium or phosphorous since oxygen was the only available reactant. The XRD of the black samples also indicated a small quantity of VO_x (Figure 5.11). The slight weight loss after 700 °C associates with degradation of vanadium and phosphorous oxides and a decrease in their oxidation states that forms other oxides like VO_2, $VO_{0.2}$, $VO_{1.27}$.

The main phases in VPP calcined are $(VO)_2P_2O_7$ and $VO(HPO_4).0.5H_2O$; in VPP equilibrated are $(VO)_2P_2O_7$; and in VPO precursor are $VO(HPO_4).0.5H_2O$ (Figure 5.11). Up to 250 °C in nitrogen, the mass of the equilibrated-catalyst, VPP calcined and VPO precursor decreased 3.65, 12.48 and 17.89 % of the original mass due to the elimination of H_2O and formation of $(VO)_2P_2O_7$ [120]. VPO precursor and VPP calcined lose both physisorbed and chemisorbed water (table 5.3 and figure 5.10), while equilibrated-catalyst only has physisorbed water to lose. VPP calcined and VPO precursor have around 5 % and 15 % of chemisorbed water in their structure. At around 300 °C, the rate of mass loss increases due to the volatilization of other chemical compounds.

XRD detected a single phase of $VO(HPO_4) \cdot 0.5\,H_2O$ in the VPO precursor. The main diffraction peaks are at 27.0°, 30.5°, 49.0°, and 63.3°, which are associated with vanadyl hydrogen phosphate hydrate (Figure 5.11 and Table 5.3).

Table 5.3 Main phases in VPP calcined, equilibrated-catalyst, and VPO precursor ($(VO)_2H_4P_2O_9$ phase is the same as $VO(HPO_4).0.5H_2O$)

Sample	Precursor	Calcined	Equilibrated
Phases	$(VO)_2H_4P_2O_9$	$(VO)_2H_4P_2O_9$ $(VO)_2P_2O_7$ $VO_{0.2}$	$(VO)_2P_2O_7$ VO_2 $VO_{1.27}$

The VPP calcined comprises two main phases of $VO(HPO_4).0.5H_2O$ ($(VO)_2H_4P_2O_9$) and $(VO)_2P_2O_7$. XRD for calcined and precursor are pretty similar, however, the peaks associated with the $(VO)_2P_2O_7$ phase are sharper, which indicates more crystallization (this is expected after calcination). This sample may contain some $VO_{0.2}$ since most peaks of $VO_{0.2}$ are confounded with peaks of the other phases in the sample. The peaks at 24.0°, 27.0°, 28.8°,

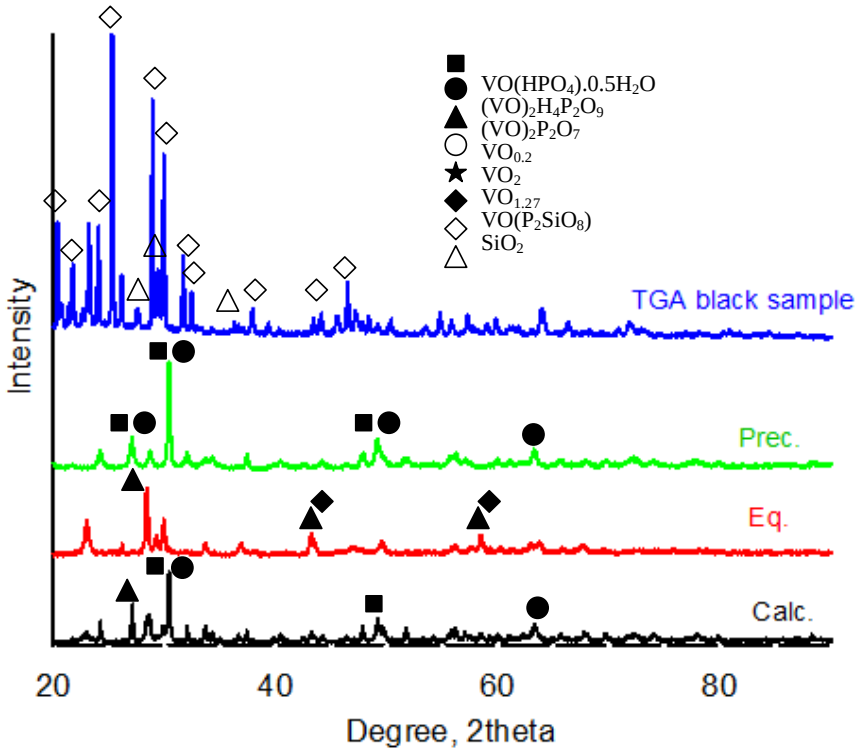

Figure 5.11 XRD pattern of VPP calcined, equilibrated-catalyst, VPO precursor and the black sample.

and 30.5°, are associated with vanadyl hydrogen phosphate hydrate and vanadyl hydrogen phosphate. The peak at 63.2° is associated with the vanadyl hydrogen phosphate phase.

The equilibrated-catalyst sample contains mainly $(VO)_2P_2O_7$, as the peaks associated with this phase are more intense than the peaks of the other phases (peaks at 28.3°, 30.0°, 43.0°, and 58.8°). The $VO(HPO_4) \cdot 0.5\,H_2O$ ($(VO)_2H_4P_2O_9$) is absent in this sample Finally, the sample contains some small quantities of VO_2 and $VO_{1.27}$ (peaks at 43.0°, 43.9°, and 58.8°).

The black sample mainly comprises $VO(P_2SiO_8)$, since the peaks associated with this phase are more intense compared to the peaks of other phases. The sample contains smaller amounts of other phases that might be $(VO)_2P_2O_7$, VOP_2O_6 and/or SiO_2 which is coherent with the SEM-EDS. The main diffraction peaks for the black sample are at 20.5°, 23.8°, and 29.0°, which are associated with vanadyl phosphate silicate. The peak at 25.2° is due to silicon oxide.

Based on XRD analysis of the four samples, almost all of the $(VO)_2H_4P_2O_9$ ($VO(HPO_4).0.5H_2O$) phase in VPP catalyst transforms to $(VO)_2P_2O_7$ phase during the partial oxidation of n-butane to maleic anhydride. Before and after the reaction (both in calcined and equilibrated VPP), $(VO)_2P_2O_7$ was the main phase. Before reaction, VPP has some $VO_{0.2}$, while after the partial oxidation (equilibrated VPP), some of the VO_2 and $VO_{1.27}$ phases appear.

VPP catalyst (precuror, calcined and equilibrated) has a mixture of V-P-O phases($(VO)_2P_2O_7$ and $VOPO_4$). Chemical bonds in these phases are similar and undifferentiable. The Calcined catalyst has a mixture of different VPO phases (Raman can detect quite small crystals that are not visible by XRD)(Figure 5.12).

The equilibrated-catalyst is more homogeneous and mainly consists of $(VO)_2P_2O_7$ (inferred from both Raman and XRD). The crystal phases of the equilibrated-catalyst does not change by increasing the temperature up to 300 °C under oxidation conditions. So, any change in the crystal structure or chemical bonds occurs at higher temperatures. In the equilibrated-catalyst, SiO_2 interacted with VPO and formed a V-Si-P-O mixed phase(Figure 5.12). According to Raman some VPO bonds are detected at ambient temperature, some VPO bonds indicate $\alpha-VOPO_4$. However, at higher temperature the bands related to $(VO)_2P_2O_7$ and V_2O_5 are small (peak at 140) due to the desgregation of VPO phases. In the black sample, V-P-O-Si phases and some incipient V_2O_5 formed that indicate that VPO phases are disaggregating (Figure 5.12).

The deactivation mechanisms during the oxidation of n-butane to maleic anhydride comprises the crystallization of amorphous phase(s) on the surface, coking and accumulation of carbonaceous species, the over-reduction of V^{4+} to V^{3+} sites or over-oxidation of V^{4+} to V^{5+}

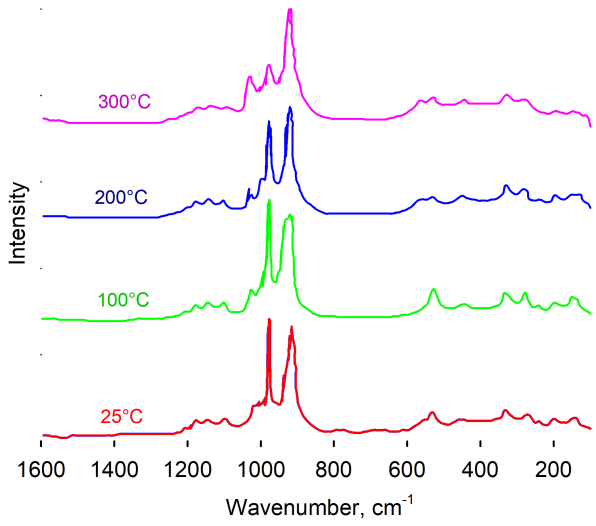

(a)

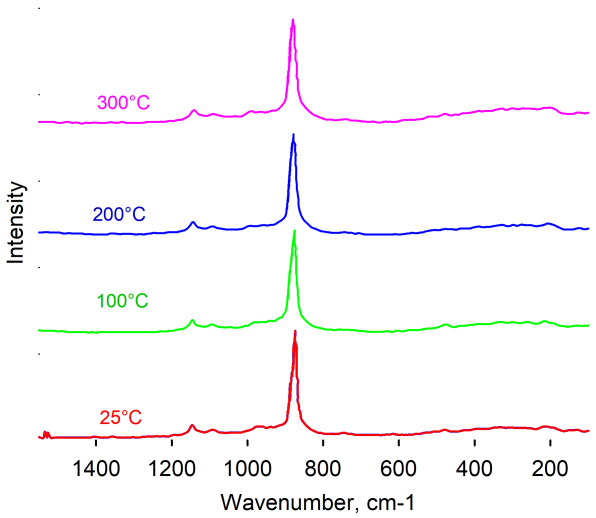

(b)

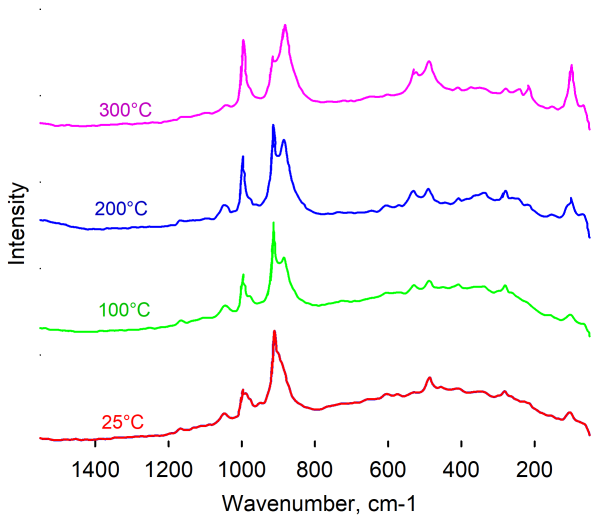

(c)

Figure 5.12 Raman spectroscopy characterization of a) VPP calcined, b) equilibrated-catalyst and c) VPO precursor

sites, loss of phosphorus, agglomeration, and sintering of the catalyst surface[121].

Effect of particle size

In all samples XRD indicates the presence of $(VO)_2P_2O_7$. $(VO)_2P_2O_7$ phase forms big crystals and aggregates while Raman recognize other phases (Raman detects smaller crystalline structures).

In 90 µm<d<120 µm has a certain degree of heterogeneity, it is mainly $(VO)_2P_2O_7$ (in accordance with XRD), but also other VPO phases (Figure 5.13). Raman recorded similar phases for d<45 µm and 24 h in steam samples (Figure 5.15 and Figure 5.16). Sample 45 µm<d<90 µm does not have such heterogeneity (both XRD and Raman detected only $(VO)_2P_2O_7$) (Figure 5.14).

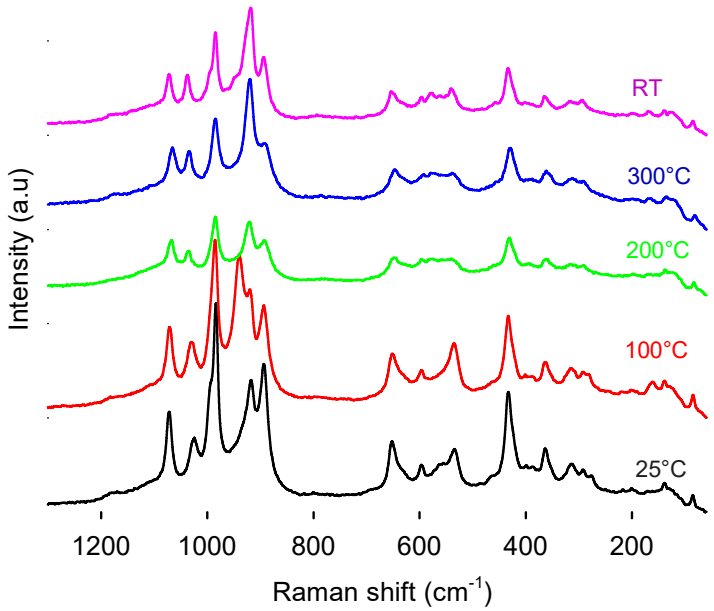

Figure 5.13 Raman spectroscopy characterization of equilibrated-catalyst of 90 µm<d<120 µm at 25, 100, 200, 300 °C and room temperature (RT)

5.5 Conclusions

In this study, we looked over the morphological changes of VPO system by temperature excursion and the partial oxidation of n-butane to maleic anhydride. TGA and XRD verified the elimination of H_2O in the equilibrated catalyst. The equilibrated-catalyst (after at least 23 days of reaction) has a smaller particle size 59 µm compared to the fresh catalyst 67 µm

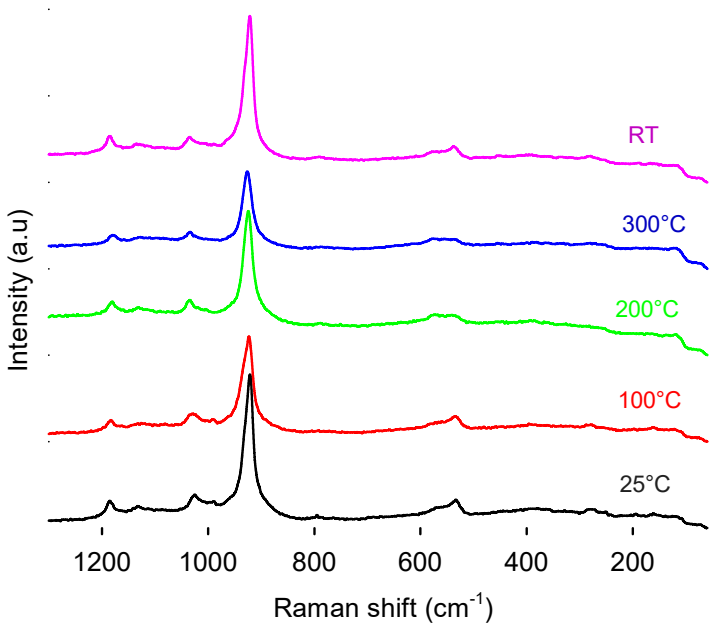

Figure 5.14 Raman spectroscopy characterization of equilibrated-catalyst of 45 µm<d<90 µm at 25, 100, 200, 300 °C and room temperature (RT)

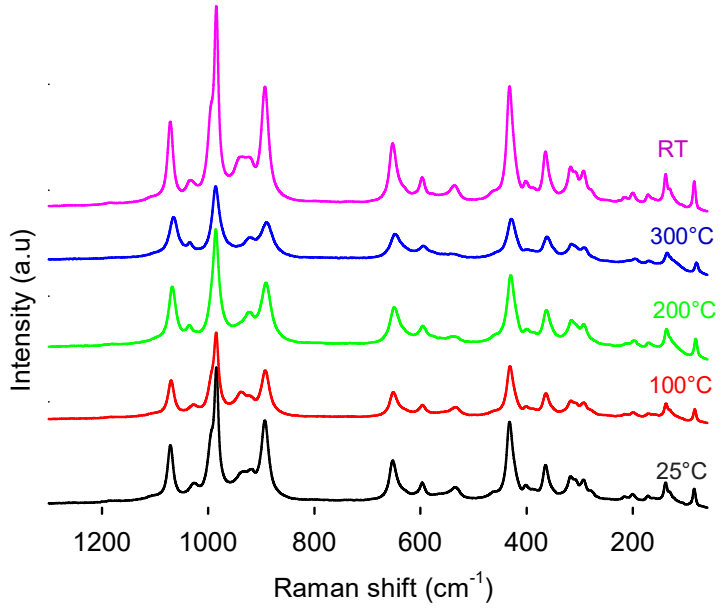

Figure 5.15 Raman spectroscopy characterization of equilibrated-catalyst of d<45 µm at 25, 100, 200, 300 °C and room temperature (RT)

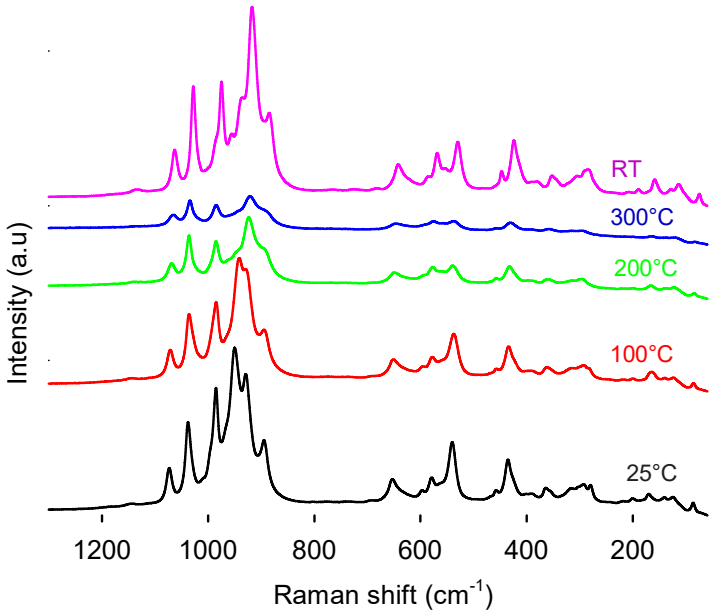

Figure 5.16 Raman spectroscopy characterization of equilibrated-catalyst after 24 h in steam at 25, 100, 200, 300 °C and room temperature (RT)

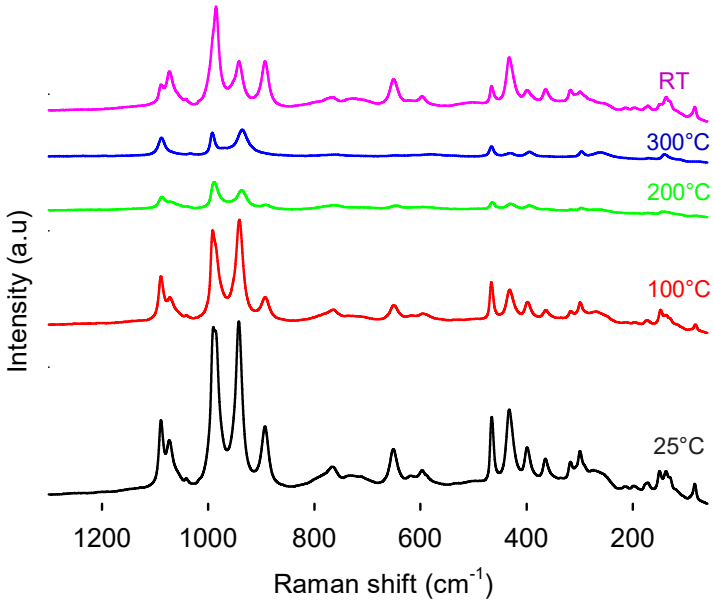

Figure 5.17 Raman spectroscopy characterization of calcined catalyst after 24 h at 789 °C in air at 25, 100, 200, 300 °C and room temperature (RT)

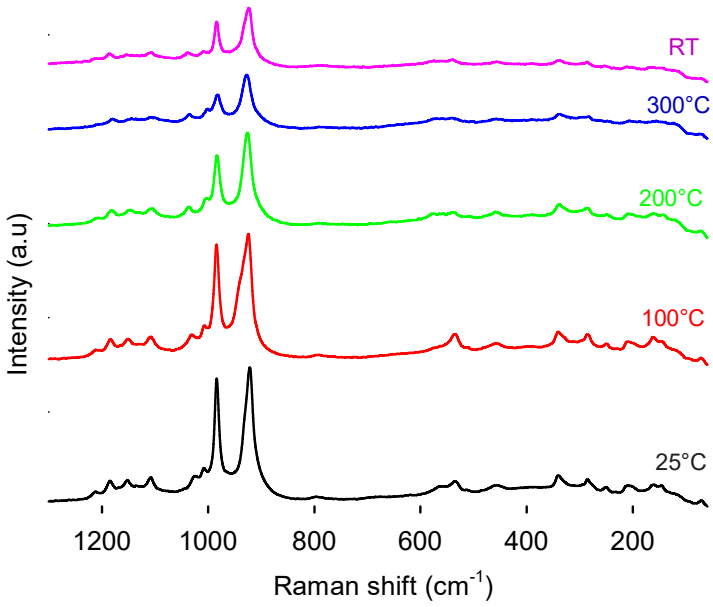

Figure 5.18 Raman spectroscopy characterization of calcined catalyst of d>120 µm at 25, 100, 200, 300 °C and room temperature (RT)

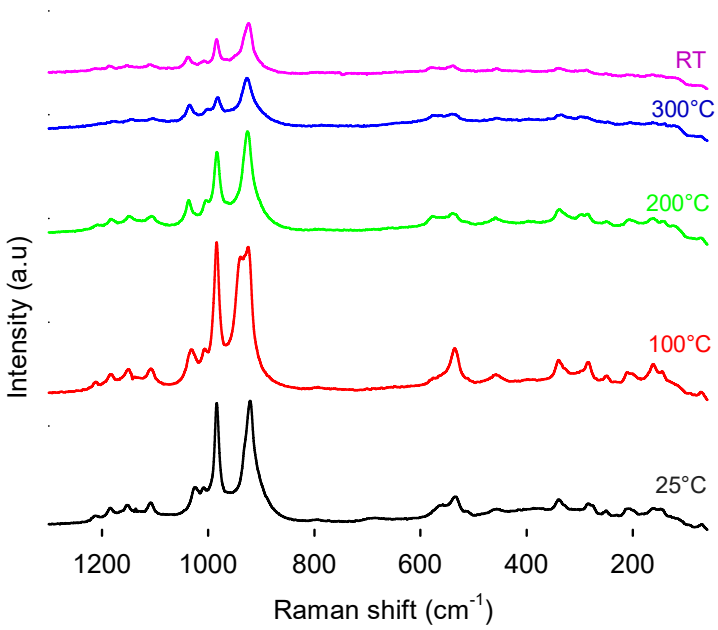

Figure 5.19 Raman spectroscopy characterization of calcined catalyst of 90 µm<d<120 µm at 25, 100, 200, 300 °C and room temperature (RT)

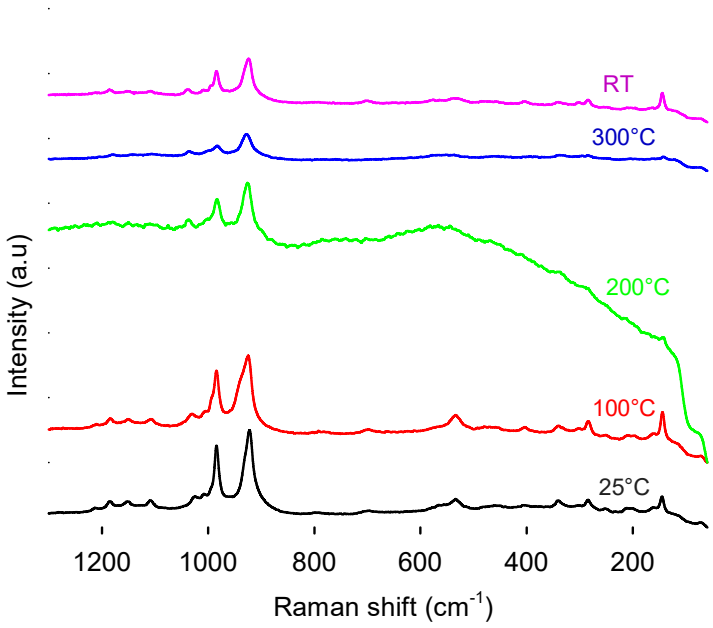

Figure 5.20 Raman spectroscopy characterization of calcined catalyst of 45 µm<d<90 µm at 25, 100, 200, 300 °C and room temperature (RT)

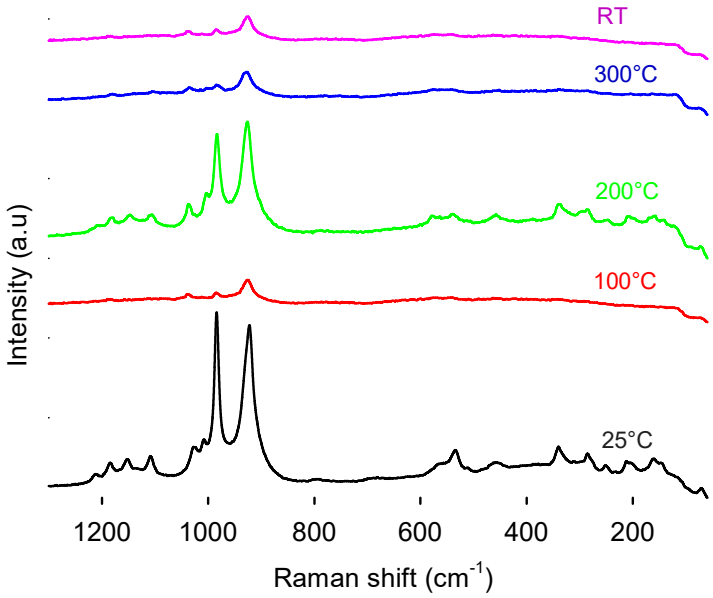

Figure 5.21 Raman spectroscopy characterization of calcined catalyst of d<45 µm at 25, 100, 200, 300 °C and room temperature (RT)

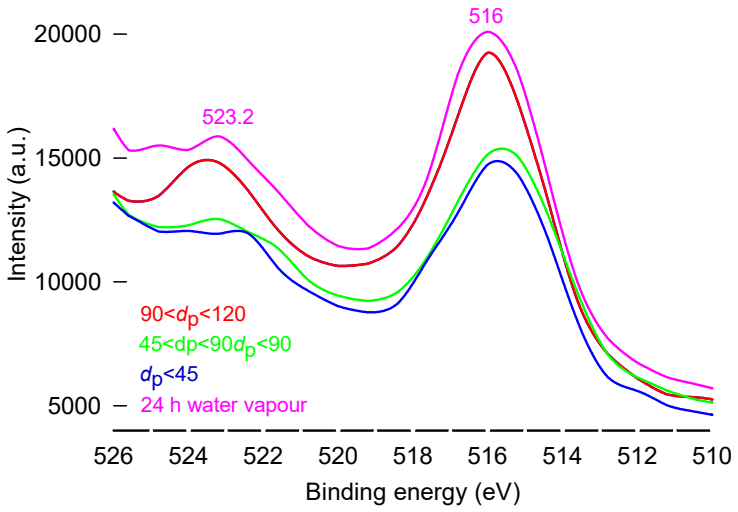

Figure 5.22 XPS spectrum of equilibrated-catalyst of d<45 µm, 45 µm<d<90 µm, 90 µm<d<120 µm, and after 24 h in steam from 530 eV to 510 eV

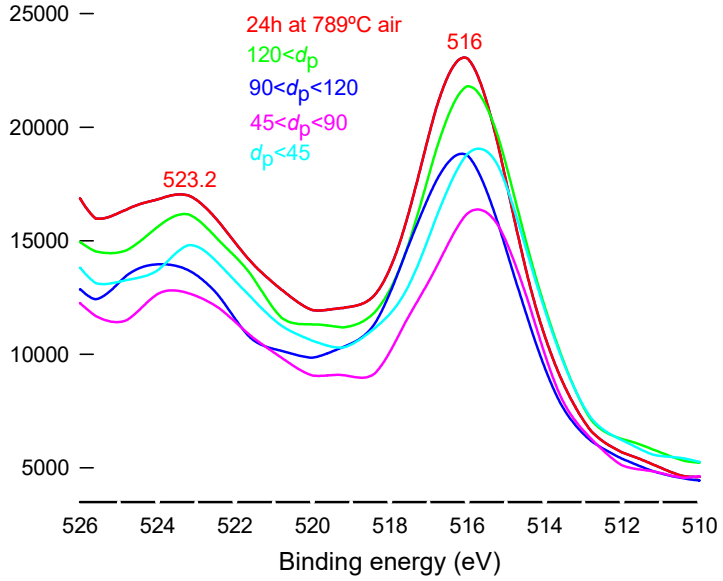

Figure 5.23 XPS spectrum of calcined-catalyst of d<45 µm, 45 µm<d<90 µm, 90 µm<d<120 µm and 120 µm<d from 530 eV to 510 eV

due to attrition[122]. The surface of the equilibrated-catalyst is smoother than that of the fresh catalyst. The precursor, calcined, and equilibrated-catalyst spherical particles turn to irregular particles in the black sample. The precursor and calcined catalyst porous surface with uniform pores (at 5000 magnifications) become smoother in the equilibrated-catalyst with less pores, and turns to a rough non-porous surface in the black sample.

The fresh catalyst has a higher pore volume ($0.14\,\mathrm{cm^3\,g^{-1}}$) compared to the equilibrated catalyst ($0.09\,\mathrm{cm^3\,g^{-1}}$), and the particle density of the catalyst increase slightly from $1713\,\mathrm{kg\,m^{-3}}$ to $1959\,\mathrm{kg\,m^{-3}}$ due to loss of porosity. Either the pores collapse they become fouled by reactants, intermediates, and/or products[123]. The silica shell in the calcined catalyst reacts with the active phase ($(VO)_2P_2O_7$) and forms $VO(P_2SiO_8)$ above 700 °C (black sample).

The specific surface area of the fresh catalyst decreased from $23\,\mathrm{m^2\,g^{-1}}$ to $12\,\mathrm{m^2\,g^{-1}}$ in the equilibrated-catalyst which due to sintering — a) crystallite growth of the catalytic phase and/or b) pore collapse on crystallites of the active phase. Sintering processes occur at high temperatures and its rate will accelerate with temperature and water. Metals sinter moderately fast in Oxygen (the VPP catalyst turned black above $710-720\,°C$ in the air)[122]. N-butane partially oxidize to MA over VPP catalyst in a fluidized bed reactor at 320 °C to 390 °C. Since sintering of VPP starts at high temperatures ($> 500\,°C$)[122], therefore the temperature in the fluidized bed would have increased. In fact, the local temperature at the sparger tips would rise above 700 °C which turns the catalyst black.

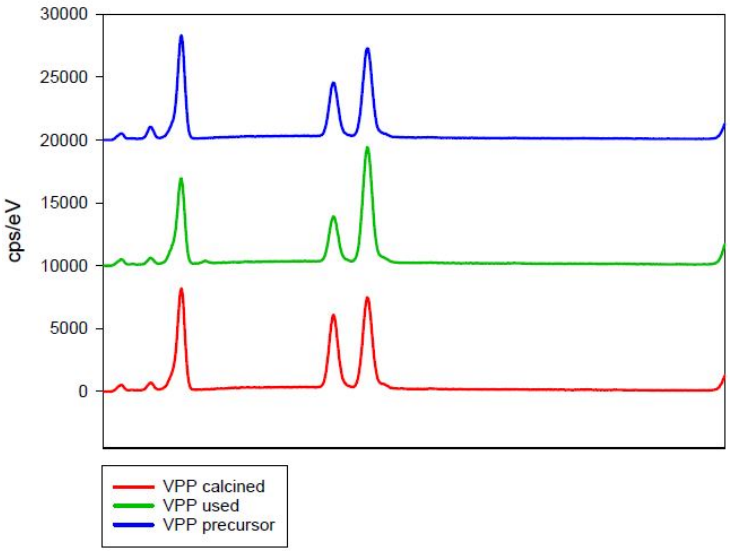

Figure 5.24 EDX spectrum of VPP calcined, equilibrated-catalyst and VPO precursor

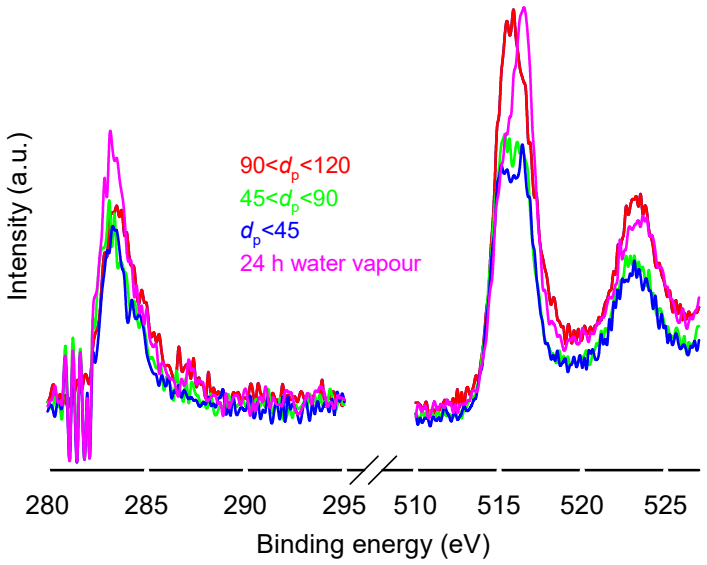

Figure 5.25 XPS spectrum of equilibrated-catalyst of d<45 µm, 45 µm<d<90 µm, 90 µm<d<120 µm, and after 24 h in steam from 280 eV to 295 eV and 510 eV to 525 eV

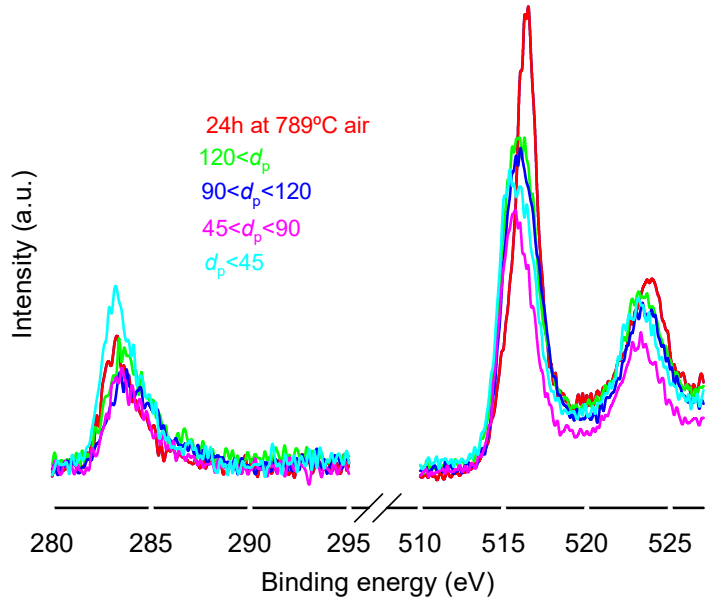

Figure 5.26 XPS spectrum of calcined-catalyst of d<45 µm, 45 µm<d<90 µm, 90 µm<d<120 µm and 120 µm<d from 280 eV to 295 eV and 510 eV to 525 eV

CHAPTER 6 GENERAL DISCUSSION

Vanadyl pyrophosphate (VPP) with a high selectivity and activity converts n-butane to maleic anhydride. DuPont commercialized a circulating fluidized bed technology for this industrially important reaction. Maleic anhydride is an organic compound, produced industrially for applications like coatings and polymers. During the reaction, the activity of VPP dropped in a short time and a fraction of the catalyst changed color from grey to black.

In this research, we characterized the catalyst physico-chemically and studied the morphological changes of the catalyst during the reaction to determine the nature of the black particles. Based on our primary hypothesis, we designed a series of experiments and analysis to achieve the research objectives. We encountered some limitations and challenges that we are explained here :

We faced many challenges during conducting several experiments to produce black sample. All the particles of vanadyl pyrophosphate catalyst did not turn black which could be due to the insufficient oxygen in contact with the fresh catalyst and/or non-uniform heat distribution during the reaction. Also, the produced black particles fused to the reactor wall so that we were not able to separate the black ones from the wall. We also tried to separate the black particles from the green ones using microscope which was unsuccessful (because of the size of the particles). To overcome these problems, we designed an experiment under a controlled condition to produce black particles in a Thermogravimetric Analyzer (TGA Q 500). The TGA recorded the mass change of the sample as a function of both increasing temperature and time. Since the capacity of the TGA pan was around 0.1 g, we had to conduct the test several times to get enough sample on for further characterized and analysis.

Despite all the limitations and challenges in experimental methodology mentioned above, we could finally produce enough amount of black sample. We observed the morphological properties of vanadyl pyrophosphate both before and after the partial oxidation of n-butane to maleic anhydride (MA). The experimental results showed that there was a decrease in both particle size and catalytic surface area of the catalyst and its surface was smoothed with no pores during the reaction. Also, the equilibtared-catalyst had a lower pore volume compared to the fresh catalyst while the particle density of the catalyst increased slightly during partial oxidation of n-butane. By sieving the equilibrated catalyst into different fractions, we observed that the smaller the particles, the darker color was the equilibrated catalyst. Although the calcined catalyst had a few black particles, but the percentage is lower than that of the the equilibrated catalyst. Moreover, the calcined catalyst had a matt texture with satellite

particles on the exterior surface, while the surface of the equilibrated catalyst particles was shiny and luminous. In addition, All samples (VPP calcined, equilibrated catalyst, and VPO precursor) have a shell of silica which covers the porous structure and some particles have hollows cores.Also, They all turned black in TGA in the presence of air, but not in nitrogen. Moreover, formation of a new crystallite phase $VO(P_2SiO_8)$ was observed and we could identify the structure and nature of the black particles in the equilibrated-catalyst (explained in detail in the discussion of the paper). The interpretations, analysis and discussions around the nature of the black particles may fill the knowledge gap in this regard.

CHAPTER 7 CONCLUSION AND RECOMMENDATIONS

This research program was related to the morphological changes of vanadyl pyrophosphate due to the thermal excursion which is an active and selective catalyst for partial oxidation of n-butane to maleic anhydride.

In the present project, we examined the effects of temperature and oxygen on VPP catalyst to study and determine the phase transformation and nature of the black particles during partial oxidation of n-butane. We also characterized the VPP catalyst, equilibrated- catalyst, VPO precursor, and the black sample to compare the changes in their properties to determine the morphological changes of the VPP catalyst during the reaction. We studied the physico-chemical properties of the samples by several analytical techniques to characterize the morphological changes. We observed that during the reaction, the VPP catalyst turned to smooth glossy non-porous surface and its particle size decreased from 67 µm to 59µm due to the attrition. The surface of the catalyst becomes smoother during the reaction. Moreover, there was a decrease in both the specific surface area and pore volume of the catalyst from 23 m^2/g and 0.14 c^3m/g to 12 m^2/g and 0.09 c^3m/g which caused by the pore collapse on crystallites of the active phase. The total surface area of the black powder is lower compared to both fresh and equilibrated catalyst which is also due to the VPO structure collapse. Also, there was an increase in the particle density of the catalyst from 1713 kg/m^3 to 1959 kg/m^3 which shows a loss of porosity. According to the obtained results, some other properties changed during the reaction for instance, the minimum fluidization velocity (Umf) of the equilibrated-catalyst (3.8 mm/s) was lower than that of The fresh catalyst (4.1mm/s) and the VPO precursor has the highest Umf (9.4mm/s) compared to the other two samples. Also, the Scott, poured, tapped density of the equilibrated catalyst are higher compared to the fresh catalyst. Moreover, the elemental analysis showed that the weight percent of both oxygen and silicon dropped during partial oxidation of n-butane, while the figure for vanadium and phosphorus increased moderately. Also, only the equilibrated catalyst possesses Fe. The elemental mapping shows some hollows cores in some particles and a silica shell with a porous structure in all three samples. We can observe satellite particles on the exterior surface of both the precursor and calcined catalyst that have a matt texture, while the surface of the equilibrated catalyst can reflect the light and has a very shiny and luminous particles. We sieved the equilibrated catalyst into different fraction and observed that the smaller particles are darker and almost 50 % of the sample with a particle size less than 45 µm possesses black samples while the figure for the sample with particles greater than 90 µm is less than 20 %. In addition,the calcined catalyst changed color to black at high temperature around 710 °C

to 720 °C in the presence of air, while it did not turn black at in nitrogen. This can suggest thermal degradation and sintering process occurred during the reaction due to an increase in temperature up to 700 °C caused by combustion at the sparger tips which turned the catalyst black.

Above 300 °C, the catalyst structure and chemical bonds change by increasing the temperature and new bond started to form and the catalytic phase $(VO)_2P_2O_7$ which is the main phase of the equilibrated catalyst transformed into a new V-Si-P-O mixed phase ($VO(P_2SiO_8)$) by SiO_2 and VPO interaction above 720 °C in the presence of air. It should be noted that, all the samples that we analyzed by a thermogravimetric analyzer, changed color to black only in the presence of air, but not in nitrogen. Analysis of the black sample shows that the VPO phases are disaggregating.

The recommendation for the future work is to produce more black sample in a well- controlled condition and conduct other characterization and analytical tests such as FTIR and ASS to better determine the nature of the black particles since the conducted experiments mostly investigated the surface of the catalysts not inside the particles. So, more data is required to provide strong evidence to show this morphology of the catalyst which caused by thermal excursion had impact on the catalyst activity. we can also do more characterization tests on the samples to see if other phenomena or parameters such as hydrocarbon radicals effect on the activity of the catalyst and how much the activity has changed. In addition, we can prepare a setup for the n-butane oxidation over both fresh catalyst and equilibrated-catalyst to determine the rate of maleic anhydride production by considering different parameters. We also recommend a sensitivity analysis to determine the effects of each involved parameters (temperature, time, gas composition) on the color change of the catalyst. For this purpose, we keep one or two parameter(s) constant to observe the effect of other variable(s) to specify which parameter(s) play(s) the most important role in this process. In the wide term, we can examine the effects of the mentioned parameters by applying a specified various time interval, test duration, heating rate, temperature ranges, gas composition (air/ N_2) to observe the properties of the sample obtained in each defined conditions.

REFERENCES

[1] F. Cavani and F. Trifiro, "The characterization of the surface properties of v- p- o-based catalysts by probe molecules," *Applied Catalysis A : General*, vol. 157, no. 1-2, pp. 195–221, 1997.

[2] K. W. Hutchenson, C. La Marca, G. S. Patience, J.-P. Laviolette, and R. E. Bockrath, "Parametric study of n-butane oxidation in a circulating fluidized bed reactor," *Applied Catalysis A : General*, vol. 376, no. 1-2, pp. 91–103, 2010.

[3] M. Witko, R. Tokarz, J. Haber, and K. Hermann, "Electronic structure of vanadyl pyrophosphate : cluster model studies," *Journal of Molecular Catalysis A : Chemical*, vol. 166, no. 1, pp. 59–72, 2001.

[4] G. S. Patience, *Experimental Methods and Instrumentation for Chemical Engineers*. Amsterdam : Elsevier, 2017.

[5] Clarivate Analytics, "Web of Science^{TM} Core Collection," 2021, accessed on 29 April 2021, http ://apps.webofknowledge.com.

[6] N. J. van Eck and L. Waltman, "Software survey : Vosviewer, a computer program for bibliometric mapping," *Scientometrics*, vol. 84, pp. 523–538, 2010.

[7] Z.-Y. Xue and G. L. Schrader, "In situ laser raman spectroscopy studies of vpo catalyst transformations," *Journal of Physical Chemistry B*, vol. 103, no. 44, pp. 9459–9467, 1999.

[8] ——, "In situ laser raman spectroscopy studies of vpo catalyst transformations," *The Journal of Physical Chemistry B*, vol. 103, no. 44, pp. 9459–9467, 1999.

[9] J. K. Bartley, N. F. Dummer, and G. J. Hutchings, "Vanadium phosphate catalysts," *Metal Oxide Catalysis*, pp. 499–537, 2008.

[10] C. J. Kiely, A. Burrows, S. Sajip, G. J. Hutchings, M. T. Sananes, A. Tuel, and J.-C. Volta, "Characterisation of variations in vanadium phosphate catalyst microstructure with preparation route," *Journal of Catalysis*, vol. 162, no. 1, pp. 31–47, 1996.

[11] Y. E. Gorbunova and S. Linde, "Structure of crystals of vanadyl pyrophosphate (vo)_2p_2o_7," in *Doklady Akademii Nauk*, vol. 245, no. 3. Russian Academy of Sciences, 1979, pp. 584–588.

[12] B. He, L. Nan, Z. Li, B. Wen, J. Niu, and R. Liu, "Effect of mo species on the selective oxidation of n-butane to maleic anhydride over mo-promoted vpp," *ChemistrySelect*, vol. 4, no. 2, pp. 662–669, 2019.

[13] N. Ballarini, F. Cavani, C. Cortelli, M. Ricotta, F. Rodeghiero, F. Trifiro, C. Fumagalli, and G. Mazzoni, "Non-steady catalytic performance as a tool for the identification of the active surface in vpo, catalyst for n-butane oxidation to maleic anhydride," *Catalysis Today*, vol. 117, no. 1-3, pp. 174–179, 2006.

[14] G. J. Hutchings, C. J. Kiely, M. T. Sananes-Schulz, A. Burrows, and J. C. Volta, "Comments on the nature of the active site of vanadium phosphate catalysts for butane oxidation," *Catalysis today*, vol. 40, no. 2-3, pp. 273–286, 1998.

[15] G. Centi, F. Trifiro, J. R. Ebner, and V. M. Franchetti, "Mechanistic aspects of maleic anhydride synthesis from c4 hydrocarbons over phosphorus vanadium oxide," *Chemical Reviews*, vol. 88, no. 1, pp. 55–80, 1988.

[16] G. Calestani, E. Cavani, A. Duran, G. Mazzoni, G. Stefani, F. Trifirò, and P. Venturoli, "Science and technology in catalysis 1994," 1995.

[17] E. Bordes, P. Courtine, and J. Johnson, "On the topotactic dehydration of vohpo4 · 0.5 h2o into vanadyl pyrophosphate," *Journal of Solid State Chemistry*, vol. 55, no. 3, pp. 270–279, 1984.

[18] G. Centi, "Vanadyl pyrophosphate-a critical overview," *Catalysis Today*, vol. 16, no. 1, pp. 5–26, 1993.

[19] L. Cornaglia, E. Lombardo, J. Andersen, and J. G. Fierro, "Acidity and catalytic behavior of vanadium-phosphorus-oxygen catalysts," *Applied Catalysis A : General*, vol. 100, no. 1, pp. 37–50, 1993.

[20] M. Abon and J.-C. Volta, "Vanadium phosphorus oxides for n-butane oxidation to maleic anhydride," *Applied Catalysis A : General*, vol. 157, no. 1-2, pp. 173–193, 1997.

[21] L. M. Cornaglia and E. A. Lombardo, "4.9 the role of acid-base and redox features in the catalytic behavior of vanadium-phosphorous-oxygen formulations," in *Studies in Surface Science and Catalysis*. Elsevier, 1994, vol. 90, pp. 429–440.

[22] G. Busca, G. Centi, F. Trifiro, and V. Lorenzelli, "Surface acidity of vanadyl pyrophosphate, active phase in n-butane selective oxidation," *Journal of Physical Chemistry*, vol. 90, no. 7, pp. 1337–1344, 1986.

[23] G. Centi, G. Golinelli, and G. Busca, "Modification of the surface pathways in alkane oxidation by selective doping of broensted acid sites of vanadyl pyrophosphate," *Journal of physical chemistry*, vol. 94, no. 17, pp. 6813–6819, 1990.

[24] W.-S. Dong, J. K. Bartley, F. Girgsdies, R. Schlögl, and G. J. Hutchings, "The hydration and transformation of vanadyl pyrophosphate," *Journal of Materials Chemistry*, vol. 15, no. 38, pp. 4147–4153, 2005.

[25] G.-U. Wolf, B. Kubias, B. Jacobi, and B. Lücke, "On the rehydration of vanadyl pyrophosphate to vanadyl hydrogenphosphate hemihydrate," *Chemical Communications*, no. 16, pp. 1517–1518, 2000.

[26] V. Guliants, J. B. Benziger, S. Sundaresan, I. Wachs, J.-M. Jehng, and J. Roberts, "The effect of the phase composition of model vpo catalysts for partial oxidation of n-butane," *Catalysis Today*, vol. 28, no. 4, pp. 275–295, 1996.

[27] F. Cavani and F. Trifiro, "The characterization of the surface properties of v- p- o-based catalysts by probe molecules," *Applied Catalysis A : General*, vol. 157, no. 1-2, pp. 195–221, 1997.

[28] G. S. Patience, R. E. Bockrath, J. D. Sullivan, and H. S. Horowitz, "Pressure calcination of vpo catalyst," *Industrial & engineering chemistry research*, vol. 46, no. 13, pp. 4374–4381, 2007.

[29] G. Mestl, D. Lesser, and T. Turek, "Optimum performance of vanadyl pyrophosphate catalysts," *Topics in Catalysis*, vol. 59, no. 17, pp. 1533–1544, 2016.

[30] R. M. Blanco, A. Shekari, S. G. Carrazán, E. Bordes-Richard, G. S. Patience, and P. Ruiz, "Significant catalytic recovery of spent industrial dupont catalysts by surface deposition of an amorphous vanadium-phosphorus oxide phase," *Catalysis today*, vol. 203, pp. 48–52, 2013.

[31] Y. Taufiq-Yap, L. Leong, M. Hussein, R. Irmawati, and S. Abd Hamid, "Synthesis and characterisation of vanadyl pyrophosphate catalysts via vanadyl hydrogen phosphate sesquihydrate precursor," *Catalysis today*, vol. 93, pp. 715–722, 2004.

[32] T. Ishimura, S. Sugiyama, and H. Hayashi, "Vanadyl hydrogenphosphate sesquihydrate as a precursor for preparation of (vo) 2p2o7 and cobalt-incorporated catalysts," *Journal of Molecular Catalysis A : Chemical*, vol. 158, no. 2, pp. 559–565, 2000.

[33] E. Bordes and P. Courtine, "Some selectivity criteria in mild oxidation catalysis : V- p-o phases in butene oxidation to maleic anhydride," *Journal of Catalysis*, vol. 57, no. 2, pp. 236–252, 1979.

[34] P. L. Gai, K. Kourtakis, D. R. Coulson, and G. C. Sonnichsen, "Hrem microstructural studies on the effect of steam exposure and cation promoters on vanadium phosphorus oxides : New correlations with n-butane oxidation reaction chemistry," *Journal of Physical Chemistry B*, vol. 101, no. 48, pp. 9916–9925, 1997.

[35] T. Tabanelli, M. Mari, F. Folco, F. Tanganelli, F. Puzzo, L. Setti, and F. Cavani, "Reactivity of vanadyl pyrophosphate catalyst in ethanol ammoxidation and β-picoline oxidation : Advantages and limitations of bi-functionality," *Applied Catalysis A : General*, vol. 619, p. 118139, 2021.

[36] N. Ballarini, F. Cavani, C. Cortelli, S. Ligi, F. Pierelli, F. Trifiro, C. Fumagalli, G. Mazzoni, and T. Monti, "Vpo catalyst for n-butane oxidation to maleic anhydride : A goal achieved, or a still open challenge ?" *Topics in catalysis*, vol. 38, no. 1-3, pp. 147–156, 2006.

[37] G. Pavarelli, J. Velasquez Ochoa, A. Caldarelli, F. Puzzo, F. Cavani, and J.-L. Dubois, "A new process for maleic anhydride synthesis from a renewable building block : The gas-phase oxidehydration of bio-1-butanol," *ChemSusChem*, vol. 8, no. 13, pp. 2250–2259, 2015.

[38] F. Wang, J.-L. Dubois, and W. Ueda, "Catalytic performance of vanadium pyrophosphate oxides (vpo) in the oxidative dehydration of glycerol," *Applied Catalysis A : General*, vol. 376, no. 1-2, pp. 25–32, 2010.

[39] G. Centi, J. Lopez-Nieto, D. Pinelli, and F. Trifiro, "Synthesis of phthalic and maleic anhydrides from n-pentane. 1. kinetic analysis of the reaction network," *Industrial & engineering chemistry research*, vol. 28, no. 4, pp. 400–406, 1989.

[40] F. Cavani, A. Colombo, F. Trifiro, M. S. Schulz, J. Volta, and G. Hutchings, "The effect of cobalt and iron dopants on the catalytic behavior of v/p/o catalysts in the selective oxidation of n-pentane to maleic and phthalic anhydrides," *Catalysis letters*, vol. 43, no. 3, pp. 241–247, 1997.

[41] B. Kerler, A. Martin, and M. Baerns, "Partial oxidation of propane to oxygenates in dense co2 phase using (vo) 2p2o7 as catalyst," *Chemical Engineering & Technology : Industrial Chemistry-Plant Equipment-Process Engineering-Biotechnology*, vol. 26, no. 4, pp. 420–424, 2003.

[42] B. Kerler, A. Martin, M.-M. Pohl, and M. Baerns, "2p2o7 catalysed partial oxidation of propane in dense co2," *Catalysis letters*, vol. 78, no. 1, pp. 259–265, 2002.

[43] A. Martin, U. Bentrup, A. Brückner, and B. Lücke, "Catalytic performance of vanadyl pyrophosphate in the partial oxidation of toluene to benzaldehyde," *Catalysis letters*, vol. 59, no. 1, pp. 61–65, 1999.

[44] U. Bentrup, A. Martin, and B. Lücke, "Infrared characterization of the surface intermediates in the oxidation of toluene on vanadyl pyrophosphate catalysts," *Topics in Catalysis*, vol. 11, no. 1, pp. 139–145, 2000.

[45] A. Caldarelli, F. Cavani, O. Garone, G. Pavarelli, J. Dubois, I. Mitsova, L. Simeonova *et al.*, "A new process for the valorisation of a bio-alcohol. the oxidehydration of 1-butanol into maleic anhydride," 2012.

[46] N. P. Rajan, G. S. Rao, B. Putrakumar, and K. V. Chary, "Vapour phase dehydration of glycerol to acrolein over vanadium phosphorous oxide (vpo) catalyst," *RSC advances*, vol. 4, no. 96, pp. 53 419–53 428, 2014.

[47] B. Katryniok, S. Paul, M. Capron, C. Lancelot, V. Bellière-Baca, P. Rey, and F. Dumeignil, "A long-life catalyst for glycerol dehydration to acrolein," *Green chemistry*, vol. 12, no. 11, pp. 1922–1925, 2010.

[48] C. Zhou, "Beltramini, jn ; fan, y.-x. ; lu, gq (max)," *Chem. Soc. Rev*, vol. 37, no. 3, p. 527, 2008.

[49] F. Wang, J.-L. Dubois, and W. Ueda, "Catalytic dehydration of glycerol over vanadium phosphate oxides in the presence of molecular oxygen," *Journal of Catalysis*, vol. 268, no. 2, pp. 260–267, 2009.

[50] U. R. Pillai and E. Sahle-Demessie, "Vanadium phosphorus oxide as an efficient catalyst for hydrocarbon oxidations using hydrogen peroxide," *New Journal of chemistry*, vol. 27, no. 3, pp. 525–528, 2003.

[51] U. Schuchardt, W. A. Carvalho, and E. V. Spinacé, "Why is it interesting to study cyclohexane oxidation ?" *Synlett*, vol. 1993, no. 10, pp. 713–718, 1993.

[52] J. N. Sarpiri, A. N. Chermahini, M. Saraji, and A. Shahvar, "Dehydration of carbohydrates into 5-hydroxymethylfurfural over vanadyl pyrophosphate catalysts," *Renewable Energy*, vol. 164, pp. 11–22, 2021.

[53] G. J. Hutchings, "Heterogeneous catalysts—discovery and design," *Journal of materials chemistry*, vol. 19, no. 9, pp. 1222–1235, 2009.

[54] A. Martin, C. Janke, and V. N. Kalevaru, "Ammoxidation of 3-picoline to nicotinonitrile over vpo catalysts," *Applied Catalysis A : General*, vol. 376, no. 1-2, pp. 13–18, 2010.

[55] E. Bordes, "Crystallochemistry of v-p-o phases and application to catalysis," *Catalysis Today*, vol. 1, no. 5, pp. 499–526, 1987.

[56] M. Ai, "Oxidation of propane to acrylic acid on v2o5&- p2o5-based catalysts," *Journal of Catalysis*, vol. 101, no. 2, pp. 389–395, 1986.

[57] G. Centi, D. Pesheva, and F. Trifiro, "Functionalization of alkanes by heterogeneous vapour-phase oxidation : Ii. propane ammoxidation," *Applied catalysis*, vol. 33, no. 2, pp. 343–359, 1987.

[58] G. Centi and F. Trifiro, "Surface kinetics of adsorbed intermediates : selective oxidation of c4- c5 alkanes," *Chemical Engineering Science*, vol. 45, no. 8, pp. 2589–2596, 1990.

[59] E. Bordes, "Nature of the active and selective sites in vanadyl pyrophosphate, catalyst of oxidation of n-butane, butene and pentane to maleic anhydride," *Catalysis Today*, vol. 16, no. 1, pp. 27–38, 1993.

[60] G. Centi, T. Tosarelli, and F. Trifiro, "Acrylonitrile from propane on (vo) 2p2o7 with preadsorbed ammonia : 1. role of competitive adsorption phenomena in determining selectivity," *Journal of Catalysis*, vol. 142, no. 1, pp. 70–83, 1993.

[61] G. Centi and F. Trifirpò, "Furan production by oxygen insertion in the 1–4 position of butadiene on vpo-based catalysts," *Journal of Molecular Catalysis*, vol. 35, no. 2, pp. 255–265, 1986.

[62] K. W. Hutchenson, C. La Marca, G. S. Patience, J.-P. Laviolette, and R. E. Bockrath, "Parametric study of n-butane oxidation in a circulating fluidized bed reactor," *Applied Catalysis A : General*, vol. 376, no. 1-2, pp. 91–103, 2010.

[63] A. Shekari, G. S. Patience, and R. E. Bockrath, "Effect of feed nozzle configuration on n-butane to maleic anhydride yield : From lab scale to commercial," *Applied Catalysis A : General*, vol. 376, no. 1-2, pp. 83–90, 2010.

[64] A. Shekari, "N-butane partial oxidation to maleic anhydride : Experimental and kinetic studies under transient conditions," Ph.D. dissertation, École Polytechnique de Montréal, 2011.

[65] G. S. Patience and R. E. Bockrath, "Butane oxidation process development in a circulating fluidized bed," *Applied Catalysis A : General*, vol. 376, no. 1-2, pp. 4–12, 2010.

[66] R. Contractor, D. Garnett, H. Horowitz, H. Bergna, G. Patience, J. Schwartz, and G. Sisler, "A new commercial scale process for n-butane oxidation to maleic anhydride using a circulating fluidized bed reactor," in *Studies in Surface Science and Catalysis*. Elsevier, 1994, vol. 82, pp. 233–242.

[67] Y. Schuurman and J. T. Gleaves, "Activation of vanadium phosphorus oxide catalysts for alkane oxidation. the influence of the oxidation state on catalyst selectivity," *Industrial & engineering chemistry research*, vol. 33, no. 12, pp. 2935–2941, 1994.

[68] G. S. Patience and M.-J. Lorences, "Vpo transient oxidation kinetics," *International Journal of Chemical Reactor Engineering*, vol. 4, no. 1, 2006.

[69] X.-F. Huang, C.-Y. Li, B.-H. Chen, and P. Silveston, "Transient kinetics of n-butane oxidation to maleic anhydride over a vpo catalyst," *AIChE journal*, vol. 48, no. 4, pp. 846–855, 2002.

[70] D. Wang and M. A. Barteau, "Kinetics of butane oxidation by a vanadyl pyrophosphate catalyst," *Journal of Catalysis*, vol. 197, no. 1, pp. 17–25, 2001.

[71] J. Gascón, R. Valenciano, C. Téllez, J. Herguido, and M. Menéndez, "A generalized kinetic model for the partial oxidation of n-butane to maleic anhydride under aerobic and anaerobic conditions," *Chemical engineering science*, vol. 61, no. 19, pp. 6385–6394, 2006.

[72] A. S. Elisabeth BORDES-RICHARDS and G. S. PATIENCE, "Oxidation catalyst," pp. 549–585, 2014.

[73] S. Mota, S. Miachon, J.-C. Volta, and J.-A. Dalmon, "Membrane reactor for selective oxidation of butane to maleic anhydride," *Catalysis today*, vol. 67, no. 1-3, pp. 169–176, 2001.

[74] M. O. Guerrero-Pérez, G. S. Patience, and M. A. Bañares, "Experimental methods in chemical engineering : Raman spectroscopy," *The Canadian Journal of Chemical Engineering*, vol. 99, no. 1, pp. 97–107, 2021.

[75] M. J. D. Mahboub, J. Wright, D. C. Boffito, J.-L. Dubois, and G. S. Patience, "Cs, v, cu keggin-type catalysts partially oxidize 2-methyl-1, 3-propanediol to methacrylic acid," *Applied Catalysis A : General*, vol. 554, pp. 105–116, 2018.

[76] N. Saadatkhah, S. Aghamiri, M. R. Talaie, and G. S. Patience, "Flame-assisted spray pyrolysis of lithium and manganese precursors to polycrystalline limn2o4," *Canadian Journal of Chemical Engineering*, vol. 97, no. 8, pp. 2299–2308, 2019.

[77] R. Schloegl, "X-ray diffraction : A basic tool for characterization of solid catalysts in the working state," *Advances in Catalysis*, vol. 52, pp. 273–338, 2009.

[78] K. Sakurai and M. Mizusawa, "X-ray diffraction imaging of anatase and rutile," *Analytical chemistry*, vol. 82, no. 9, pp. 3519–3522, 2010.

[79] H. Stanjek and W. Häusler, "Basics of x-ray diffraction," *Hyperfine interactions*, vol. 154, no. 1, pp. 107–119, 2004.

[80] J. Epp, "X-ray diffraction (xrd) techniques for materials characterization," in *Materials characterization using nondestructive evaluation (NDE) methods*. Elsevier, 2016, pp. 81–124.

[81] Z. Ye, X. Jiang, and Z. Wang, "Measurements of particle size distribution based on mie scattering theory and markov chain inversion algorithm." *J. Softw.*, vol. 7, no. 10, pp. 2309–2316, 2012.

[82] C. A. L. y Leon, "New perspectives in mercury porosimetry," *Advances in colloid and interface science*, vol. 76, pp. 341–372, 1998.

[83] A. Abell, K. Willis, and D. Lange, "Mercury intrusion porosimetry and image analysis of cement-based materials," *Journal of colloid and interface science*, vol. 211, no. 1, pp. 39–44, 1999.

[84] F. Ambroz, T. J. Macdonald, V. Martis, and I. P. Parkin, "Evaluation of the bet theory for the characterization of meso and microporous mofs," *Small Methods*, vol. 2, no. 11, p. 1800173, 2018.

[85] M. Viana, P. Jouannin, C. Pontier, and D. Chulia, "About pycnometric density measurements," *Talanta*, vol. 57, no. 3, pp. 583–593, 2002.

[86] G. S. Bumbrah and R. M. Sharma, "Raman spectroscopy–basic principle, instrumentation and selected applications for the characterization of drugs of abuse," *Egyptian Journal of Forensic Sciences*, vol. 6, no. 3, pp. 209–215, 2016.

[87] P. Gabbott, *Principles and applications of thermal analysis*. John Wiley & Sons, 2008.

[88] A. Coats and J. Redfern, "Thermogravimetric analysis. a review," *Analyst*, vol. 88, no. 1053, pp. 906–924, 1963.

[89] A. Mandal, M. Sarkar, and D. Bhattacharya, "A simple edxrf technique to analyse alloys," *The European Physical Journal-Applied Physics*, vol. 17, no. 1, pp. 81–84, 2002.

[90] S. Piorek, "Principles and applications of man-portable x-ray fluorescence spectrometry," *TrAC Trends in Analytical Chemistry*, vol. 13, no. 7, pp. 281–286, 1994.

[91] A. H. Pinto, "Portable x-ray fluorescence spectrometry : principles and applications for analysis of mineralogical and environmental materials," *Asp. Min. Miner. Sci*, vol. 1, pp. 42–47, 2018.

[92] N. Gurker, M. F. Ebel, and H. Ebel, "Imaging xps—a new technique, i—principles," *Surface and interface analysis*, vol. 5, no. 1, pp. 13–19, 1983.

[93] J. K. Bartley, N. F. Dummer, and G. J. Hutchings, "Vanadium phosphate catalysts," *Metal Oxide Catalysis*, pp. 499–537, 2008.

[94] V. Guliants, J. B. Benziger, S. Sundaresan, N. Yao, and I. Wachs, "Evolution of the active surface of the vanadyl pyrophosphate catalysts," *Catalysis Letters*, vol. 32, no. 3, pp. 379–386, 1995.

[95] G. Mestl, D. Lesser, and T. Turek, "Optimum performance of vanadyl pyrophosphate catalysts," *Topics in Catalysis*, vol. 59, no. 17, pp. 1533–1544, 2016.

[96] M. Heenemann, C. Heine, M. Hävecker, A. Trunschke, and R. Schlögl, "Influence of steam on a vanadyl pyrophosphate catalyst during propane oxidation," *Journal of Physical Chemistry B*, vol. 122, no. 2, pp. 695–704, 2018.

[97] E. Bordes, "Reactivity and crystal chemistry of vpo phases related to c4-hydrocarbon catalytic oxidation," *Catalysis Today*, vol. 3, no. 2-3, pp. 163–174, 1988.

[98] ——, "Crystallochemistry of v-p-o phases and application to catalysis," *Catalysis Today*, vol. 1, no. 5, pp. 499–526, 1987.

[99] G. S. Patience, R. E. Bockrath, J. D. Sullivan, and H. S. Horowitz, "Pressure calcination of vpo catalyst," *Industrial & Engineering Chemistry Research*, vol. 46, no. 13, pp. 4374–4381, 2007.

[100] J. W. Johnson, D. C. Johnston, A. J. Jacobson, and J. F. Brody, "Preparation and characterization of vanadyl hydrogen phosphate hemihydrate and its topotactic transformation to vanadyl pyrophosphate," *Journal of the American Chemical Society*, vol. 106, no. 26, pp. 8123–8128, 1984.

[101] G. Centi, D. Pesheva, and F. Trifiro, "Functionalization of alkanes by heterogeneous vapour-phase oxidation : Ii. propane ammoxidation," *Applied catalysis*, vol. 33, no. 2, pp. 343–359, 1987.

[102] G. S. Patience and R. E. Bockrath, "Butane oxidation process development in a circulating fluidized bed," *Applied Catalysis A : General*, vol. 376, no. 1-2, pp. 4–12, 2010.

[103] A. Shekari, G. S. Patience, and R. E. Bockrath, "Effect of feed nozzle configuration on n-butane to maleic anhydride yield : From lab scale to commercial," *Applied Catalysis A : General*, vol. 376, no. 1-2, pp. 83–90, 2010.

[104] R. M. Contractor, "Dupont's cfb technology for maleic anhydride," *Chemical Engineering Science*, vol. 54, no. 22, pp. 5627–5632, 1999.

[105] G. Centi, G. Golinelli, and F. Trifiro, "Nature of the active sites of (vo) 2p2o7 in the selective oxidation of n-butane : Evidence from doping experiments," *Applied Catalysis*, vol. 48, no. 1, pp. 13–24, 1989.

[106] M. Abon and J.-C. Volta, "Vanadium phosphorus oxides for n-butane oxidation to maleic anhydride," *Applied Catalysis A : General*, vol. 157, no. 1-2, pp. 173–193, 1997.

[107] J. Ebner and M. Thompson, "An active site hypothesis of well-crystallized vanadium phosphorus oxide catalyst systems," *Catalysis today*, vol. 16, no. 1, pp. 51–60, 1993.

[108] A. M. Wernbacher, M. Eichelbaum, T. Risse, S. Cap, A. Trunschke, and R. Schlögl, "Operando electrical conductivity and complex permittivity study on vanadia oxidation catalysts," *Journal of Physical Chemistry C*, vol. 123, no. 13, pp. 8005–8017, 2018.

[109] W. R. Moser, *Advanced catalysts and nanostructured materials : modern synthetic methods*. Academic press, 1996.

[110] E. Bordes, P. Courtine, and J. Johnson, "On the topotactic dehydration of vohpo4 · 0.5 h2o into vanadyl pyrophosphate," *Journal of Solid State Chemistry*, vol. 55, no. 3, pp. 270–279, 1984.

[111] G. S. Patience and E. Bordes-Richard, "International VPO Workshop : Preface," *Applied Catalysis A : General*, vol. 376, no. 1-2, pp. 1–3, 2010.

[112] M. R. Thompson, C. Tzoganakis, and G. L. Rempel, "Functionalization of ethylene-propylene-diene terpolymer via the alder ene reaction," *Polymer Engineering and Science*, vol. 38, no. 10, pp. 1694–1707, 1998.

[113] P. Wongthong, C. Nakason, Q. M. Pan, G. L. Rempel, and S. Kiatkamjornwong, "Styrene-assisted grafting of maleic anhydride onto deproteinized natural rubber," *European Polymer Journal*, vol. 59, pp. 144–155, 2014.

[114] ——, "Modification of deproteinized natural rubber via grafting polymerization with maleic anhydride," *European Polymer Journal*, vol. 49, no. 12, pp. 4034–4046, 2013.

[115] N. Saadatkhah, M. G. Rigamonti, D. C. Boffito, H. Li, and G. S. Patience, "Spray dried sio2 wo3/tio2 and sio2 vanadium pyrophosphate core-shell catalysts," *Powder Technology*, vol. 316, pp. 434–440, 2017.

[116] P. Amorós, R. Ibáñez, E. Martínez-Tamayo, A. Beltrán-Porter, D. Beltrán-Porter, and G. Villeneuve, "New vanadyl hydrogenphosphate hydrates. electronic spectra of the vo2+ ion in the vo (hxpo4) x · yh2o system," *Materials research bulletin*, vol. 24, no. 11, pp. 1347–1360, 1989.

[117] H. Li, M. Rostamizadeh, K. Mameri, D. C. Boffito, N. Saadatkhah, M. G. Rigamonti, and G. S. Patience, "Ultrasound assisted wet stirred media mill of high concentration lifepo4 and catalysts," *Canadian Journal of Chemical Engineering*, vol. 97, no. 8, pp. 2242–2250, 2019.

[118] M. G. Rigamonti, Y.-X. Song, H. Li, N. Saadatkhah, P. Sauriol, and G. S. Patience, "Influence of atomization conditions on spray drying lithium iron phosphate nanoparticle suspensions," *Canadian Journal of Chemical Engineering*, vol. 97, no. 8, pp. 2251–2258, 2019.

[119] R. Bardestani, G. S. Patience, and S. Kaliaguine, "Experimental methods in chemical engineering : specific surface area and pore size distribution measurements—bet, bjh, and dft," *Canadian Journal of Chemical Engineering*, vol. 97, no. 11, pp. 2781–2791, 2019.

[120] J. Do, R. P. Bontchev, and A. J. Jacobson, "Vanadyl oxalatophosphate compounds (c2h10n2)[vo (hpo4)] 2 (c2o4) and (ch6n3) 2 [[vo (hpo4)] 2 (c2o4) and their thermal transformation to (vo) 2p2o7 via vohpo4," *Chemistry of materials*, vol. 13, no. 8, pp. 2601–2607, 2001.

[121] R. M. Blanco, A. Shekari, S. G. Carrazán, E. Bordes-Richard, G. S. Patience, and P. Ruiz, "Significant catalytic recovery of spent industrial dupont catalysts by surface deposition of an amorphous vanadium-phosphorus oxide phase," *Catalysis Today*, vol. 203, pp. 48–52, 2013.

[122] C. H. Bartholomew, "Mechanisms of catalyst deactivation," *Applied Catalysis A : General*, vol. 212, no. 1-2, pp. 17–60, 2001.

[123] M. D. Argyle and C. H. Bartholomew, "Heterogeneous catalyst deactivation and regeneration : a review," *Catalysts*, vol. 5, no. 1, pp. 145–269, 2015.